AD-A126 875 STUDY OF FATIQUE MECHANISMS IN AEROSPACE STRUCTURAL MATERIALS(U) SOUTHWEST RESEARCH INST SAN ANTONIO TX J LANKFORD ET AL. FEB 83 AFOSR-TR-83-0207 1/1

UNCLASSIFIED F49620-78-C-0022 F/G 11/4 NL

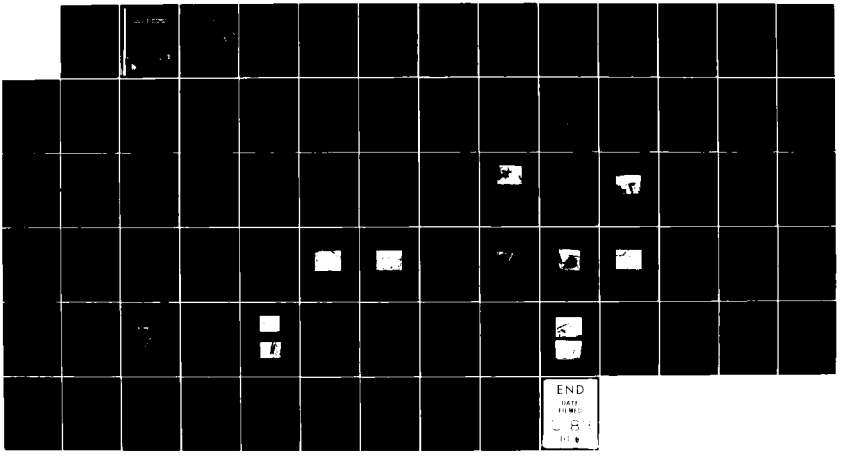

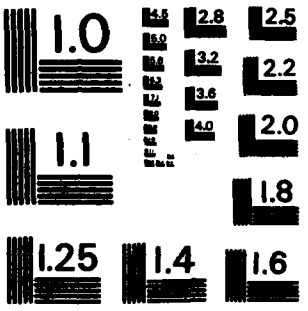

MICROCOPY RESOLUTION TEST CHART
NATIONAL BUREAU OF STANDARDS-1963-A

AFOSR-TR - 83 - 0209

SwRI-5159

AD A126875

STUDY OF FATIGUE MECHANISMS IN AEROSPACE STRUCTURAL MATERIALS

by

James Lankford
David L. Davidson
Gerald R. Leverant

AFOSR FINAL REPORT

Period January 1978 to December 1982

This research was sponsored by the Air Force Office of Scientific Research, Directorate of Electronics and Solid State Sciences, Under Contract F49620-78-C-0022

Approved for release; distribution unlimited.

February 1983

DTIC FILE COPY

DTIC ELECTE APR 14 1983 S D H

SOUTHWEST RESEARCH INSTITUTE
SAN ANTONIO HOUSTON

83 04 14 020

AFOSR-TR- 83-0207

SwRI-5159

STUDY OF FATIGUE MECHANISMS IN AEROSPACE STRUCTURAL MATERIALS

by

James Lankford
David L. Davidson
Gerald R. Leverant

AFOSR FINAL REPORT

Period January 1978 to December 1982

DTIC
APR 14 1983
H

This research was sponsored by the Air Force Office of Scientific Research,
Directorate of Electronics and Solid State Sciences,
Under Contract F49620-78-C-0022

Approved for release; distribution unlimited.

February 1983

Approved:

U.S. Lindholm, Director
Department of Materials Sciences

AIR FORCE OFFICE OF SCIENTIFIC RESEARCH (AFSC)
NOTICE OF TRANSMITTAL TO DTIC
This technical report has been reviewed and is
approved for public release IAW AFR 190-12.
Distribution is unlimited.
MATTHEW J. KERPER
Chief, Technical Information Division

UNCLASSIFIED

SECURITY CLASSIFICATION OF THIS PAGE (When Data Entered)

REPORT DOCUMENTATION PAGE		READ INSTRUCTIONS BEFORE COMPLETING FORM
1. REPORT NUMBER AFOSR-TR- 83-0207	2. GOVT ACCESSION NO. AD-A126 875	3. RECIPIENT'S CATALOG NUMBER
4. TITLE (and Subtitle) Study of Fatigue Mechanisms in Aerospace Structural Materials		5. TYPE OF REPORT & PERIOD COVERED Final Scientific Report 1 Jan 1978 - 31 Dec 1982
		6. PERFORMING ORG. REPORT NUMBER 06-5159
7. AUTHOR(s) James Lankford David L. Davidson Gerald R. Leverant		8. CONTRACT OR GRANT NUMBER(s) F49620-78-C-0022
9. PERFORMING ORGANIZATION NAME AND ADDRESS Southwest Research Institute 6220 Culebra Road (P.O. Drawer 28510) San Antonio, TX 78284		10. PROGRAM ELEMENT, PROJECT, TASK AREA & WORK UNIT NUMBERS 61102F 2306/A1
11. CONTROLLING OFFICE NAME AND ADDRESS AF Office of Scientific Research Bolling AFB, Building 410 Washington, DC 20332 /NE		12. REPORT DATE February 1983 13. NUMBER OF PAGES 77
14. MONITORING AGENCY NAME & ADDRESS(if different from Controlling Office)		15. SECURITY CLASS. (of this report) UNCLASSIFIED 15a. DECLASSIFICATION/DOWNGRADING SCHEDULE

16. DISTRIBUTION STATEMENT (of this Report)

Approved for public release; distribution unlimited

17. DISTRIBUTION STATEMENT (of the abstract entered in Block 20, if different from Report)

18. SUPPLEMENTARY NOTES

19. KEY WORDS (Continue on reverse side if necessary and identify by block number)

Fatigue	Titanium Matrix Composites
Crack Initiation	Hydrogen Embrittlement
Crack Growth	Crack Tip Plasticity
Aluminum	Overloads
Titanium	Dwell Debit

20. ABSTRACT (Continue on reverse side if necessary and identify by block number)

This report summarizes the results of a five-year, three-phase study of (1) fatigue crack growth and load interaction modeling in aluminum alloys, (2) the effect of microstructure on susceptibility to hydrogen embrittlement in titanium alloys, and (3) micromechanisms of fatigue crack growth in titanium matrix composites.

DD FORM 1473 EDITION OF 1 NOV 65 IS OBSOLETE

UNCLASSIFIED

SECURITY CLASSIFICATION OF THIS PAGE (When Data Entered)

1. Aluminum Alloy Task

In the aluminum phase of the work, special new techniques, including electron channeling, cycling of specimens within the SEM and, stereoimaging analysis of crack tips, have been applied to the problem of determining critical crack tip parameters. Displacement fields have been mapped out, and load spectrum effects have been interpreted in terms of crack tip residual stresses and crack closure. New information of importance in modeling the fatigue crack growth mechanism has been obtained; in particular, details of crack tip yielding have been determined which indicate that the crack growth process is much more complicated than generally envisioned. Plastic zone size and shape and the distribution of strain within the plastic zone were determined for the high-strength aluminum alloys 2024-T4, 6061-T6, and 7075-T6 using the technique of selected area electron channeling. Plastic zone size was found to correlate with the work done in creating a unit of new crack surface and the yield stress, rather than with the stress intensity factor and yield stress. Plastic strain distribution was found to be a logarithmic function of distance from the crack tip, in agreement with the mathematical analysis for a moving crack in plane strain. However, it was found that for these alloys, the actual crack tip plastic zone size strain parameters are not predicted by current theory. Crack tip strains obtained experimentally, through stereoimaging analysis, have been used to evaluate which of several possible failure criteria (strain range, stress range, critical strain to fracture, cumulative damage, and critical work to failure) should be incorporated into a realistic crack growth model. It was found that only the critical strain to fracture model was compatible with all of the observed crack tip parameters. In addition, progress has been made in developing computational codes for transforming crack tip strains into the corresponding local stress fields; these results can be used in determining the residual stress fields caused by overloads.

2. Titanium Alloy Task

The titanium alloy task was primarily concerned with identifying the mechanism responsible for the reduction in low-cycle fatigue life of beta processed titanium alloys under dwell conditions at peak load. Recommendations for minimizing or eliminating the dwell debit using microstructural control were made based on the research. In the final year of the project, a small subtask was undertaken to evaluate the feasibility of developing a dual microstructure alloy that was optimized for both fatigue crack initiation and propagation resistance.

The effect of dwell periods at peak load was studied on five near-alpha and alpha-beta alloys. Variables which were examined included type of loading, hydrogen content, beta-phase distribution, time to failure and creep strain. It was found that the large reduction in fatigue life during dwell cycling was due to an internal hydrogen embrittlement phenomenon. The embrittlement occurs by localized increases in hydrogen content at the tips of long, blocked shear bands developed during time-dependent plastic deformation. The key microstructural features responsible for the embrittlement process have been determined to be large transformed beta colony size and a fine, discontinuous distribution of beta phase within the colony. Alpha-beta alloys that contain thick, continuous beta platelets were determined to be immune to embrittlement.

With the objective of producing a fine-grained, fatigue crack initiation resistant surface layer on a coarse-grained, fatigue crack growth resistant core, heavy cold working of the surface of beta-annealed Ti-6Al-4V specimens was performed by shot peening. Subsequently, recrystallization heat treatments were conducted. Although, some success was achieved in the recrystallization of a thin surface layer, the recrystallized zone was very non-uniform. This was apparently due to the heterogeneous nature of the deformation in the coarse-grained beta-annealed material and the more extensive cold work at the specimen corners during peening.

3. Titanium Matrix Composite Task

In the titanium matrix composite phase, the effect of the strength of the interface between fiber and matrix has been investigated. It was found that decreasing the strength of this interface greatly changes the process by which a fatigue crack moves through the material; crack growth along the interfaces becomes much more important, and the minimum applied stress intensity factor at which fatigue cracks will grow is increased. Interfacial shear strength is decreased by heat treatment, and this occurs because of the segregation of calcium to the interface. A model has been developed to relate interfacial calcium content to heat treatment parameters.

Fiber strengths were measured after being removed from the composite, and a statistical variation of strengths were found, which were independent of length of the fiber. Microscopic examination of the fibers confirmed that they had been altered due to the processing steps accompanying manufacture of the composite.

Crack tip strains were measured for a crack in the matrix and in the as-received composite, both remote and local to the fibers. Equivalent cyclic stress intensity factors in the composite were derived from measured crack tip strains, and from this, crack growth rates were derived, which agreed well with measured values. Average fatigue crack growth through the composite has been modeled taking into account the various factors affecting the growth rate, even though the "average" situation occurs with considerable uncertainty.

Accession For
NTIS GRA&I
DTIC TAB
Unannounced
Justification
By
Distribution/
Availability Codes
Dist | Avail and/or Special
A

FOREWORD

This report summarizes work carried out under a five-year program to investigate several critical technological problems associated with fatigue crack growth in aerospace structural alloys. The program was divided into three major tasks, dealing with aluminum, titanium, and titanium-matrix composite materials, respectively.

The aluminum alloy task was focused primarily upon two related problems. In the first case, the dependence of crack extension upon microstructural parameters is a prerequisite for designing new, or modifying old, alloys in order to achieve greater fatigue resistance. Thus, effort was directed towards learning how, on a microscopic scale, fatigue cracks actually extend. In particular, it was desired to establish local crack tip failure criteria. Achievement of this goal required the development of special, new experimental techniques.

The second area of concern under this task was the critical problem of predicting the fatigue lifetimes of flawed (cracked) structures subject to the variable amplitude load spectra characteristic of in-service flight. It is well known that random stress overloads lead to the phenomenon of crack growth retardation, while underloads may either accelerate crack extension during subsequent constant amplitude cycling, or counteract the beneficial effect of a previous overload.

In order to properly address this problem, changes in local crack tip conditions wrought by particular types of loading must be taken into account. Specifically, it is necessary to characterize the extent of the crack tip plastic zone due to the loading, and the stress-strain conditions prevailing within this zone, which serve as input parameters in current load spectrum crack growth models. These factors are all functions of alloy chemistry and microstructure, hence, both ingot and powder metallurgy alloys of varying chemistry were studied.

There is a continuing interest in the beta processing of near-alpha and alpha-beta titanium alloys for several reasons. A major incentive is cost reduction because of the lower press load requirements and superior shape definition achievable by processing these alloys at a temperature above the beta transus. In addition, increases in creep resistance, fracture toughness, and fatigue crack propagation resistance can be obtained with the large colony microstructure developed during beta processing. The large colony microstructure consists of colonies of aligned alpha platelets in a matrix of beta. The beta is present as a thin film at the alpha platelet boundaries. Increases in fatigue crack propagation resistance and fracture toughness have been attributed to an increase in crack path tortuosity brought about by the deflection of a moving crack along the alpha-beta interfaces present in the colonies.

Recently, however, it has been found that the introduction of a five-minute dwell period at peak loads approaching the yield stress can reduce the low-cycle fatigue life of smooth specimens by two orders of magnitude in Ti-6Al-5Zr-0.5Mo-0.25Si (IMI-685) with a large colony microstructure. In addition, the percent elongation was reduced to 50 pct of that obtained in a tensile test. The goals of the present work included the determination of the microstructural features which control the embrittlement process. A model was developed which can be applied to beta-annealed titanium alloys in general.

Also, fatigue crack initiation resistance is generally compromised by a large colony and/or prior beta-grain size. It would be desirable, therefore, to develop a dual microstructure for optimum fatigue resistance, particularly for applications involving stress concentrations where surface crack initiation is common. A fine-grained surface layer combined with a coarse-grained underlayer could be very resistant to crack initiation at the surface, but, if a crack did initiate, the coarse-grained interior could significantly retard the crack propagation rate. An exploratory subtask was initiated in the final year of the program to determine whether such a dual microstructure could be achieved in a manner compatible with standard fabrication techniques.

Metal matrix composites are being developed for specialized structural applications in both airframes and engines. To date, most of the mechanical properties work on this class of materials has been aimed at tensile strength, even though these materials will be used in environments where cyclic loading is important. The focus of this task has been to examine in detail how fatigue cracks move through composites of titanium matrix with boron carbide coated boron fibers, and to understand how the interface between the matrix and fiber controls crack growth. Some of the questions we have attempted to answer are: How strong should the matrix/fiber interface be for best fatigue crack growth rate resistance? What is the effect of thermal treatment, such as might be used in forming these materials, on fatigue crack growth resistance? Can we derive mathematical models for the growth of fatigue cracks through this class of materials? Answers to these questions would benefit both designers who wish to utilize these materials and future efforts to design better metal matrix composites.

TABLE OF CONTENTS

LIST OF ILLUSTRATIONS

LIST OF ILLUSTRATIONS (CONTINUED)

LIST OF ILLUSTRATIONS (CONTINUED)

I. ALUMINUM ALLOY TASK

David L. Davidson and James Lankford

A. Research Objectives

1. Develop an understanding of the mechanism of fatigue crack propagation in aluminum alloys through study of the damaged material in the immediate crack tip vicinity.
2. Determine the mechanism(s) by which transient loading conditions (overloads, underloads) modify steady-state fatigue crack growth, and quantify the microstructural and plasticity parameters which control this effect.
3. Establish the physical bases (criteria) for crack advance.
4. Develop models for crack growth under steady-state and transient loading conditions based on crack tip metallurgical and micromechanical considerations.

B. Summary of Research Effort

During the last five years, the authors have been engaged in the study of fatigue crack tip yielding and micromechanics in aluminum alloys. This work is detailed in some twenty-five technical papers (Section), hence the present summary permits a complete description of neither the unusual techniques employed, nor of all the results. The purpose here is to outline the experimental approach, discuss the major achievements of the program, and put both in perspective.

Two principal experimental techniques have been employed. The first, selected area electron channeling, has been used to map out the shapes and extents crack tip plastic zone, and also as a semiquantitative strain measurement. Knowledge of these factors is extremely important, since they relate to the description of cracks by the methods of linear elastic fracture mechanics, as well as to theoretical studies describing crack tip mechanics.

Strain distributions about fatigue crack tips in aluminum alloys 7075-T6, 2024-T4, and 6061-T6 were exhaustively mapped out using selected area electron channeling.[1] Systematic changes in channeling patterns caused by cyclic deformation near fatigue crack tips was quantified for each alloy using tensile calibration specimens.[2] This permitted the determination of strain distributions for various angular orientations about the crack tip, from the plastic zone boundary to within as close as 10-20 μm of the actual tip. This is much closer to the tip than deformation has heretofore been measured. Typical results, representing numerous specimens, are shown for an orientation of 45° for 2024-T4 in Figure 1; also shown are the strain distributions according to LEFM[3] and a non-linear power law-hardening[4] material. It can be seen that the total strain ε_t rises rather rapidly as one progresses toward the crack tip from the plastic zone boundary to a distance of 10-20 μm from the tip. This strain should represent that which is attained during the actual loading portion of the fatigue cycling process. Experimental results, minus data points, are collected in Figure 2 for all three alloys studied, at $\theta = 45°$. These curves have the general form

$$\varepsilon_t = \varepsilon_o - m\ln(r + A) \tag{1}$$

where ε_o, m, and A are constants, in qualitative agreement with Rice's theoretical analysis[5] for a stable, moving crack.

For such alloys, it has been previously thought that the plastic zone shapes should be similar, and the maximum size r_p, corresponding to the 0.2% yield strength σ_y, should be given[3] by

$$r_p = \alpha\left(\frac{K_{max}}{\sigma_y}\right)^2 \tag{2}$$

where K_{max} is the maximum value of the cyclic stress intensity, and α is supposed to be an alloy-independent constant.

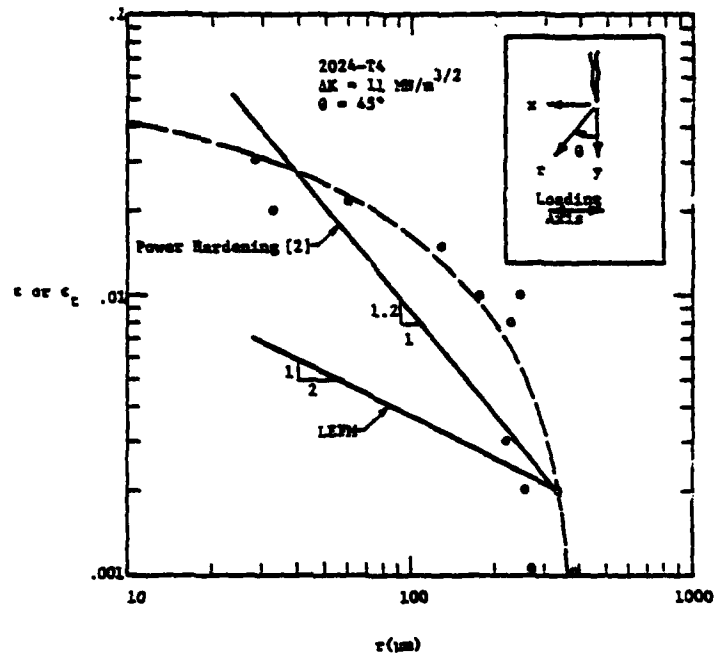

Figure 1. Equivalent Tensile Strain Vs Distance from the Crack Tip at θ = 45° for 2024-T4.

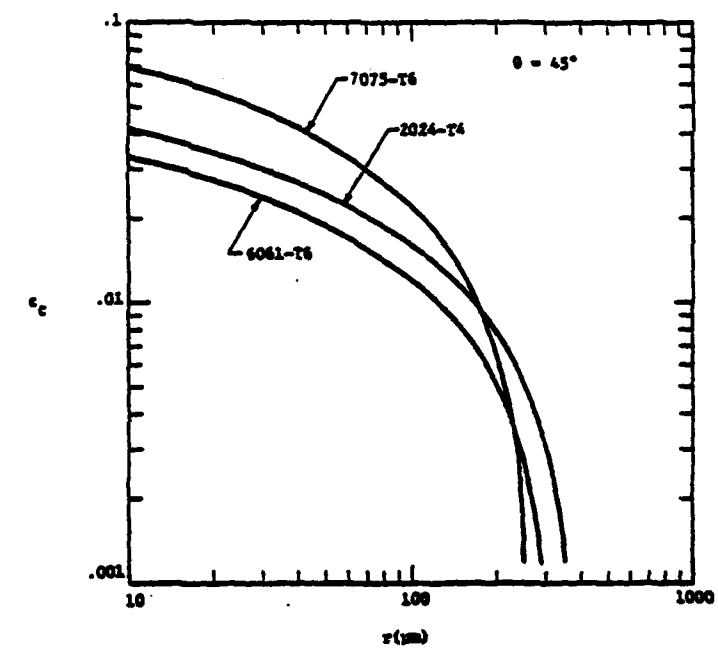

Figure 2. Equivalent Tensile Strain Vs Distance from Crack Tip at θ = 45° for All Three Alloys.

Relative shapes and sizes of the plastic zones for the three alloys are shown in Figure 3. Comparison shows differences in the shapes, but the average sizes, surprisingly, are much the same, even though the yield stresses for the materials vary widely. Normalizing these plastic zones according to Eq. (2), yields maximum values of α which are approximately 0.37, 0.2 and 0.76 for 2024-T4, 6061-T6 and 7075-T6 respectively[6] (Figure 4). In addition, these maxima do not occur at the same angular orientation, since the fundamental shapes of the isostrain contours are distinctly different for the three materials.

These results were successfully normalized quantitatively on the basis of a plastic work model.[7] Since the plastic zone sizes could not be accounted for via yield strength [Eq. (1)], r_p was rederived in terms of $\frac{dW}{dA}$, the work absorbed by the specimen as an incremental area of new crack surface, dA, is created by the external cyclic force. Analysis showed that while the plastic zone sizes are <u>not</u> proportional to $(\frac{K_{max}}{\sigma_y})^2$, they <u>are</u> proportional to

$$\frac{\frac{dW}{dA}\,E}{\sigma_y^{\,2}}$$

where E is Young's modulus. Further analysis was developed which linked total cumulative strain and cyclic strain range, and indicated that the equivalent tensile strains should exceed the cyclic strain range, particularly in the outer region of the plastic zone.

All of these results had implications regarding the modification of the crack tip driving force (ΔK) following overloads, but they did not explain the basis for cyclic crack extension per se. In particular, knowledge of yielding and crack tip micromechanics within the critical, highly strained region lying with ~20 μm of the crack tip was required. However, concurrent research during the same period led to the discovery of a new method of visualizing crack tip plasticity, which was subsequently developed

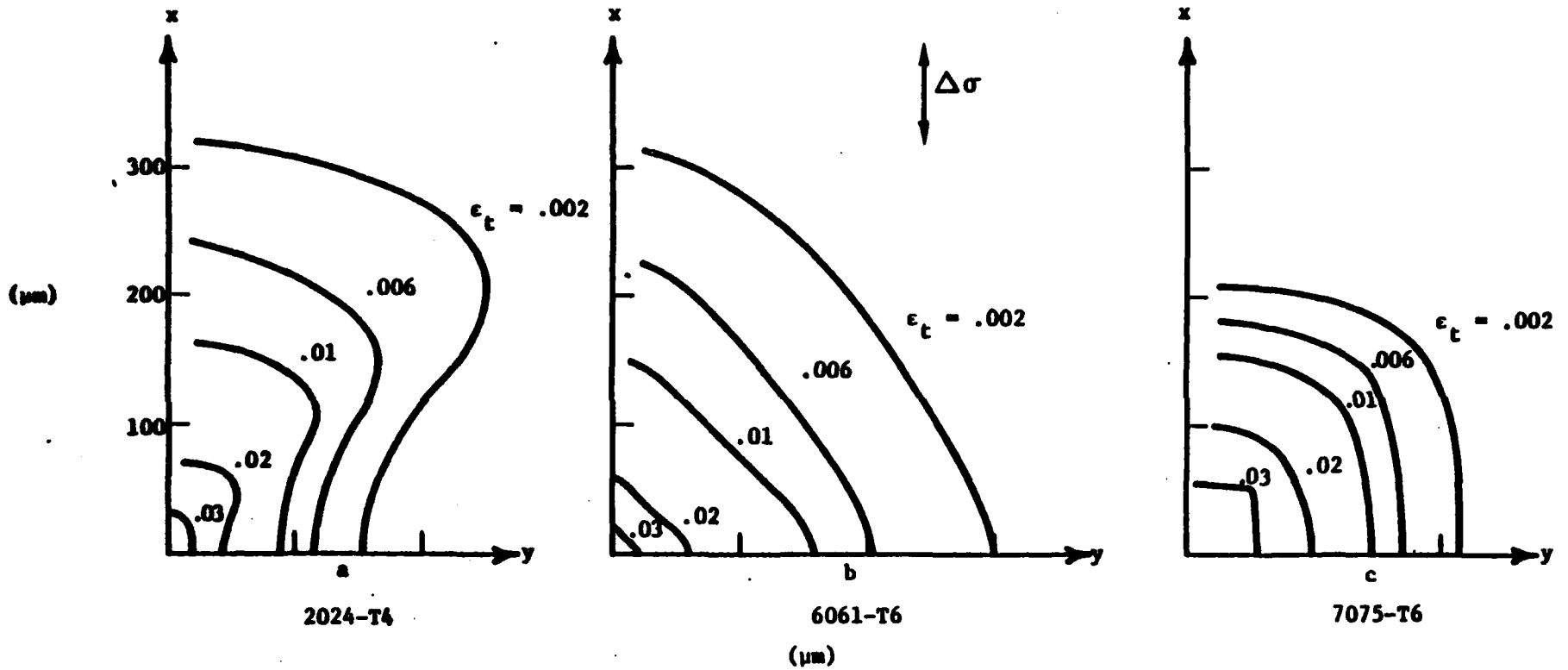

Figure 3. Plastic Zone Size.

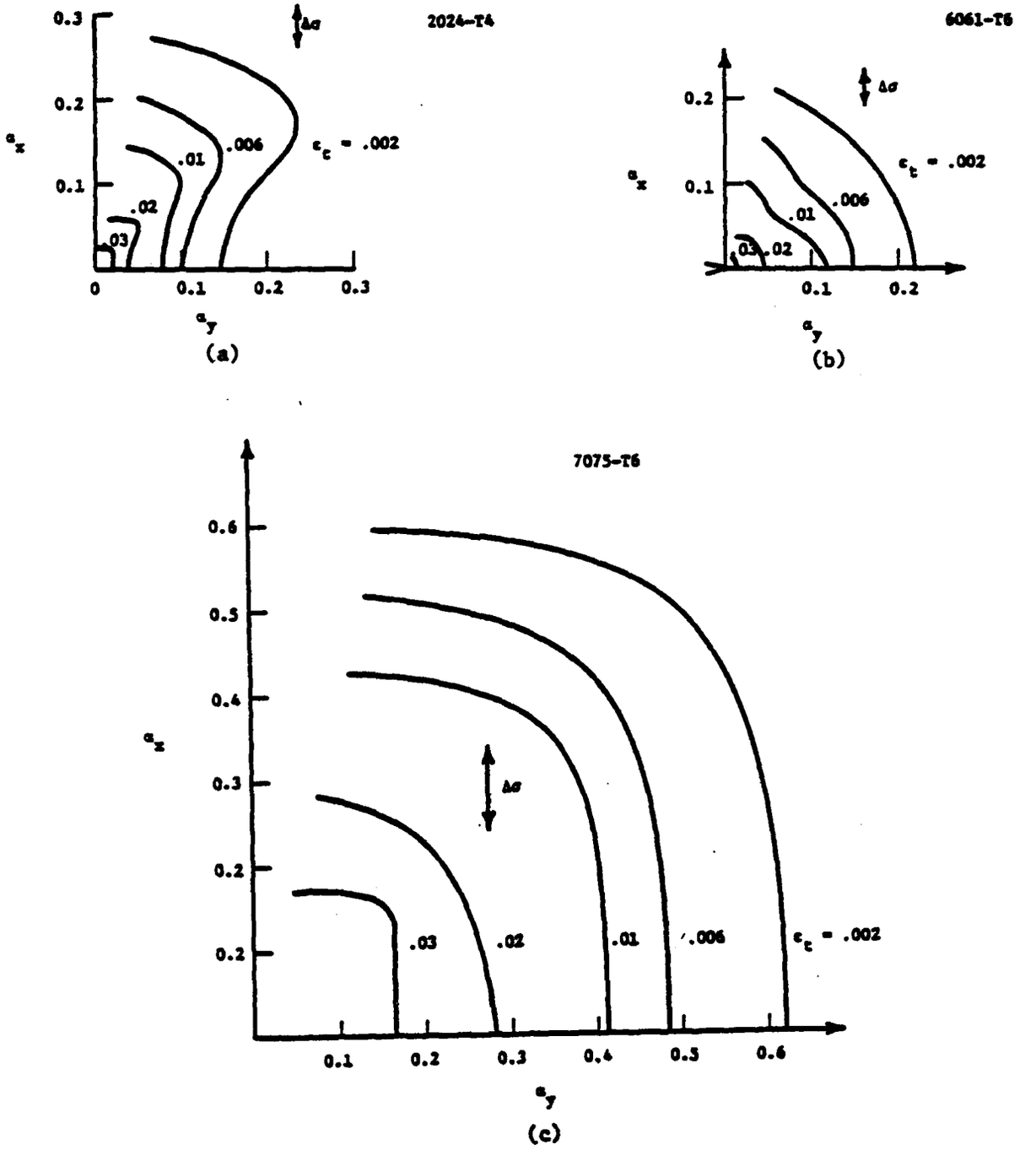

Figure 4. Reduced Plastic Zone Dimension $\alpha(= {}^{r_p}/_{(K/\sigma_y)^2}$.

to the extent that very accurate quantitative measurement of material displacements have now been carried out to within less than one micrometer of the crack tip. The technique involves obtaining pairs of photographs, at identical magnification, of crack tips in two different states of loading; in our work, the photographs are generated by means of a special cyclic loading stage within the SEM specimen chamber. By inspecting the photos in a stereoviewer, the crack tip displacements may be discerned.[8,9] Moreover, use of quantitative photogrammetry permits actual measurement of the displacements (Figure 5), while rotation of the photos in the viewer resolves the displacement field into orthogonal components, i.e., the directions of the principal displacements are revealed. Spatial differentiation of the results yields the crack tip strain field; Figure 6 shows two different ways of displaying this data.[10-12]

On the basis of such measurements, considerable progress has been made in modeling fatigue crack growth. It should be noted that this progress has derived from additional ancillary experiments carried out under dynamic observational conditions[13,14] using the SEM cycling stage. In particular, for various aluminum alloys at relatively low stress intensities, it has become increasingly clear that crack extension does not occur on every cycle. Instead, as cycling progresses, the tip generally blunts to an ever increasing extent (but does not grow), while the crack tip opening likewise increases, until the crack extends upon reaching some critical state, which our data suggest corresponds to a critical cumulative strain.[15] This sharp-blunt growth sequence is then repeated.

With this fact in mind, two new fatigue crack growth models have been developed.[15] The first is based on a cumulative strain concept, in which the near-crack tip element is treated as a tiny low-cycle fatigue specimen. However, the low-cycle fatigue law which governs its failure is derived by direct determination of several crack tip parameters, including the ΔK dependence of the crack tip plastic strain range $\Delta\varepsilon_p$ (Figure 7) and the crack opening displacement, COD (Figure 8). These factors can be combined to yield a crack growth law of the form

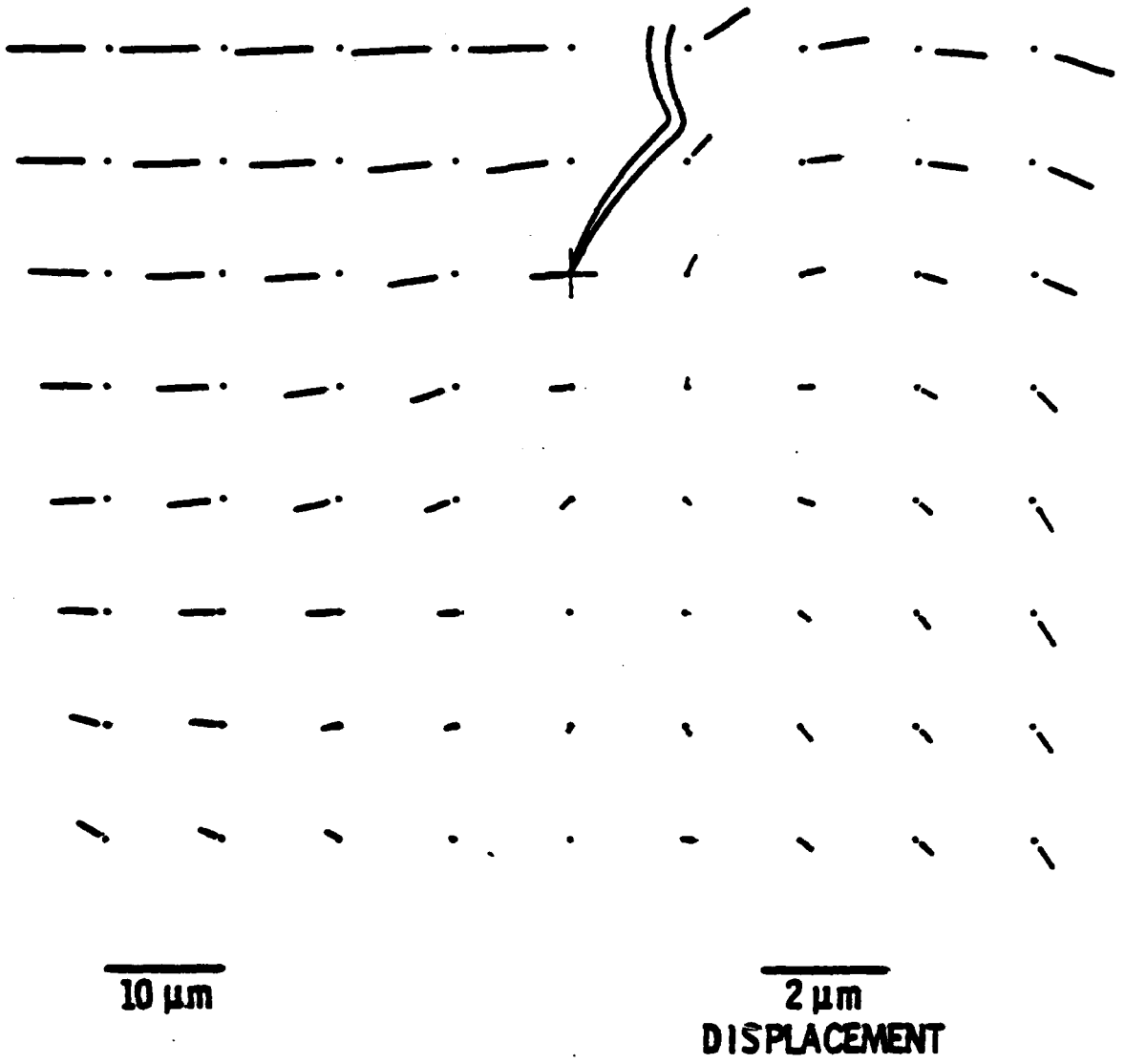

Figure 5. Displacements Measured from Stereopair Photomicrographs. Notice that the length of the displacements is magnified relative to the spatial distances shown. The dot marks the undeformed location and the end of the line displacement due to the loading increment.

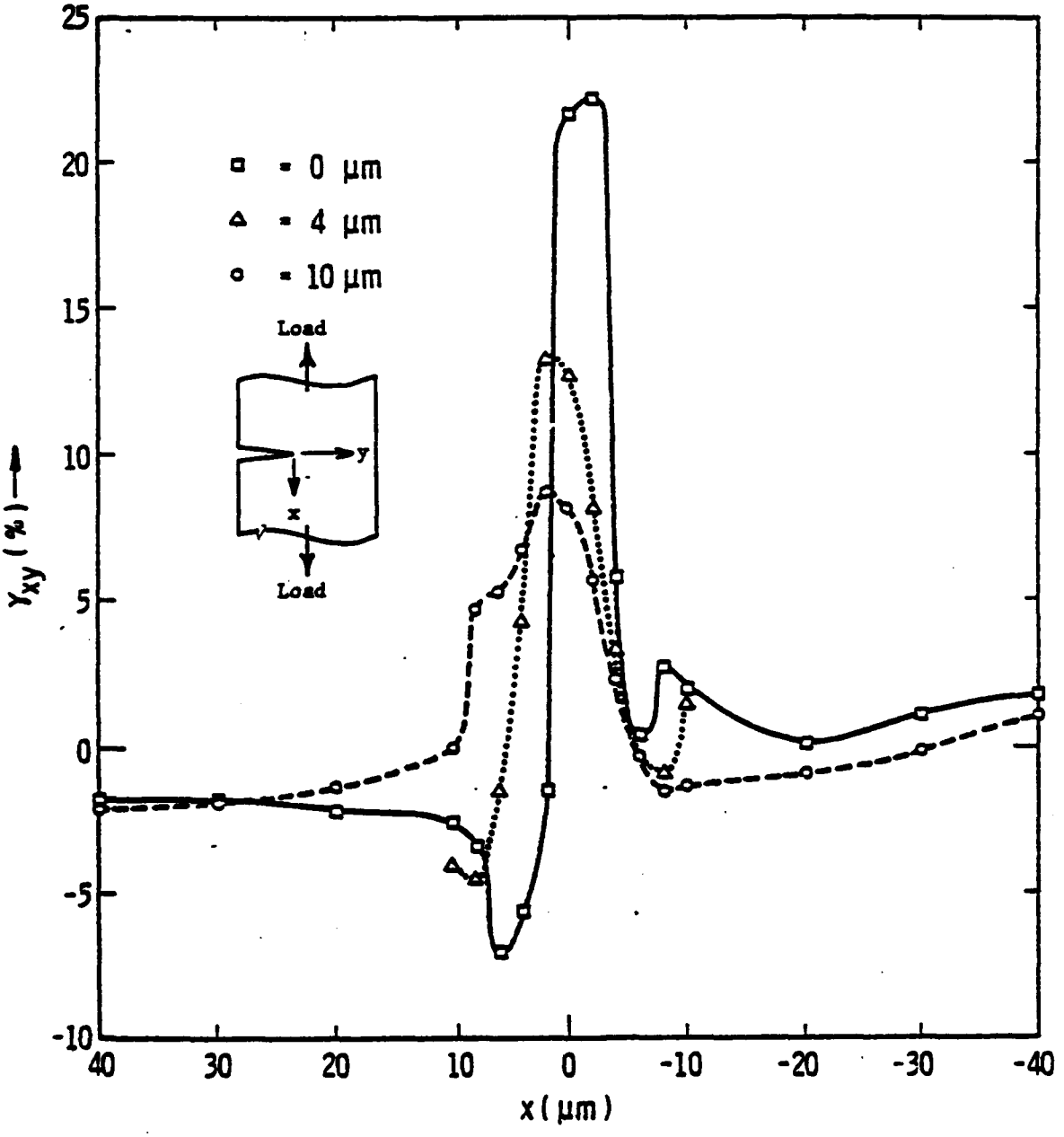

Figure 6A. Shear Strain Versus Distance (x) Normal to the Crack for Several Values of Distance (y) Ahead of the Crack. Material is MA-87 aluminum.

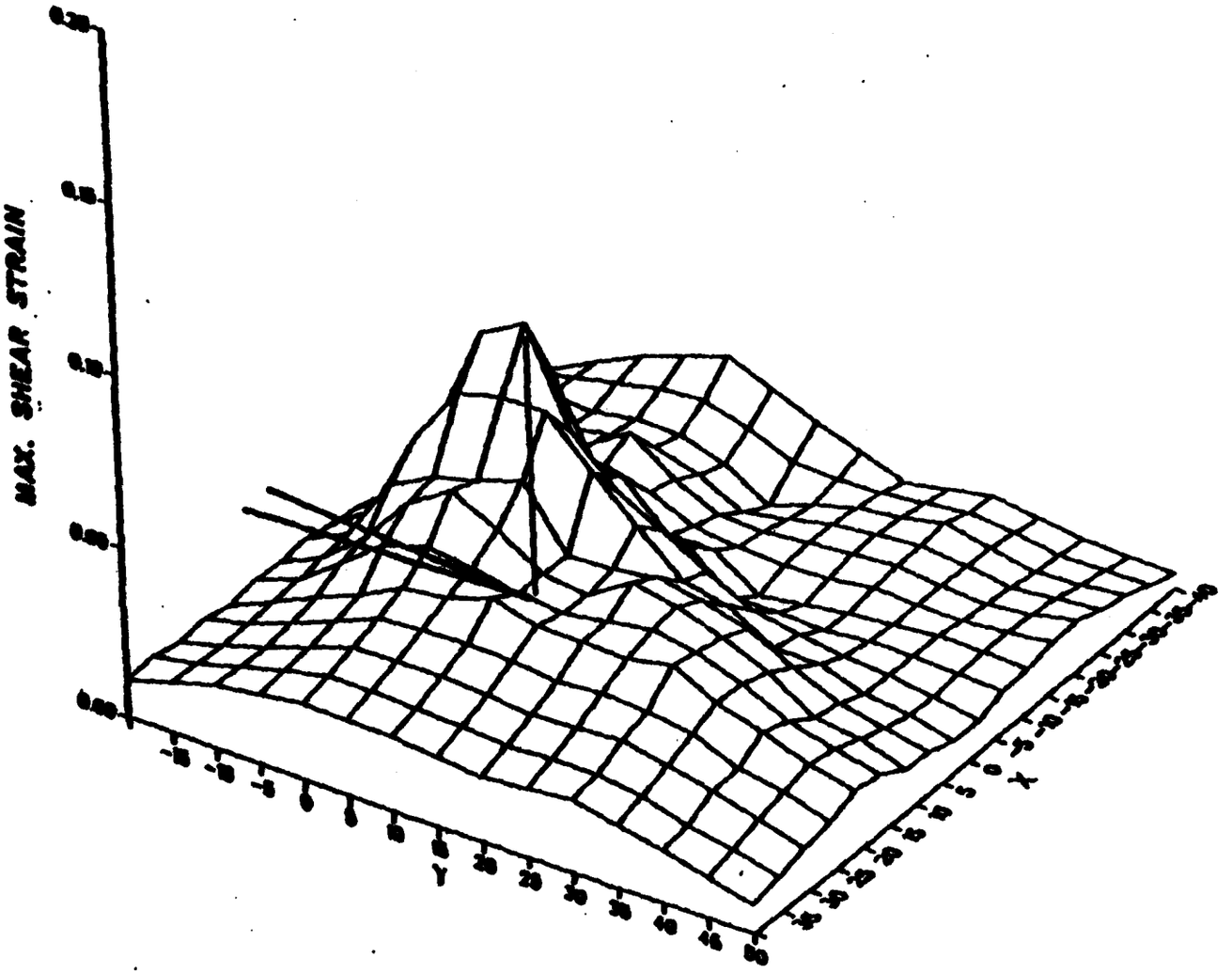

Figure 6B. Maximum Values of the Strains Derived from a Displacement Field. Distances along the x and y axes are in micrometers. The crack is shown schematically on the plane of zero strain.

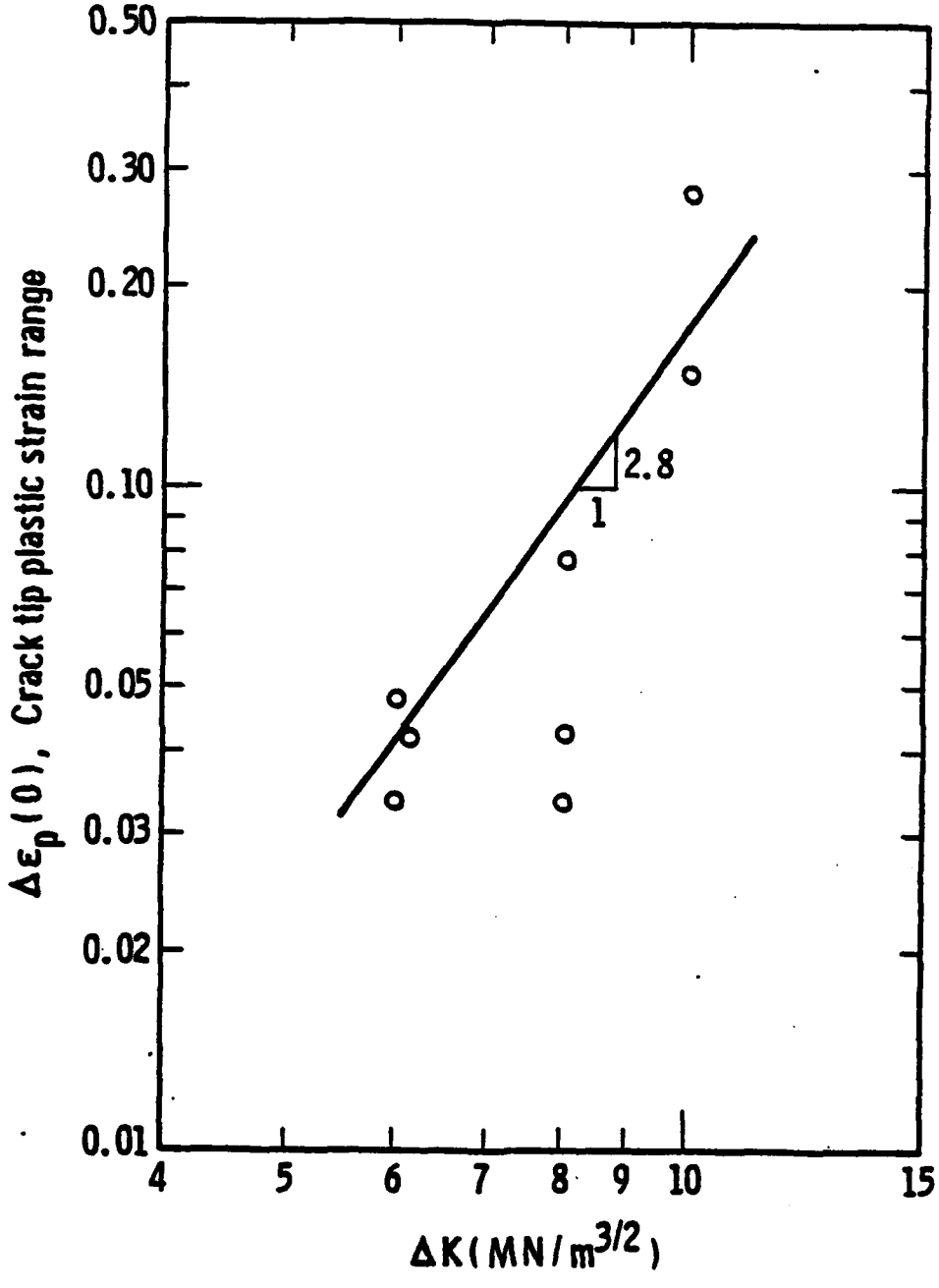

Figure 7. Crack Tip Plastic Strain Range Vs ΔK; The Line Shown is Consistent with the Critical Strain Model.

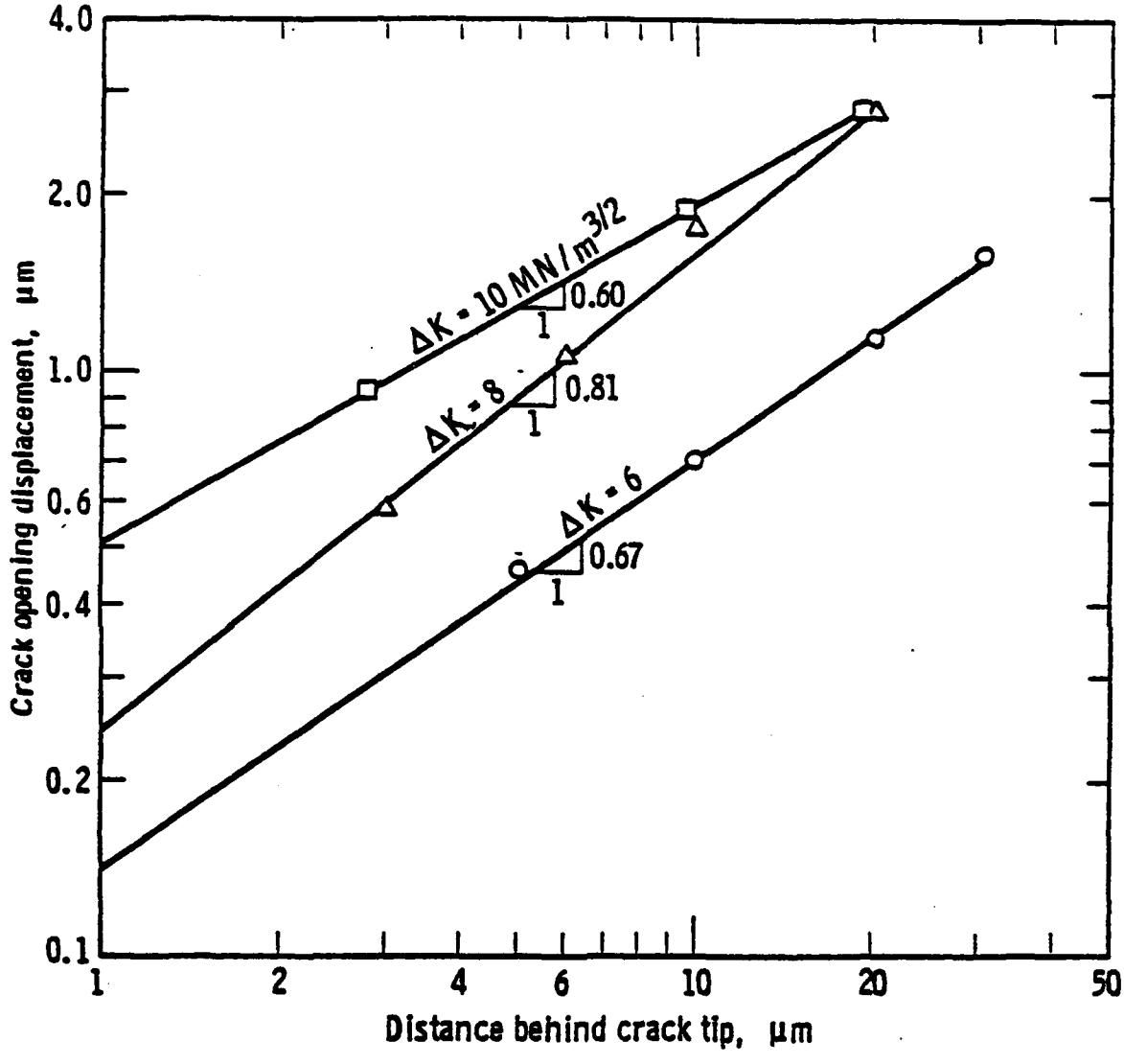

Figure 8. Crack Opening Displacement as a Function of Distance Behind the Crack Tip.

$$\frac{da}{dN} = \frac{\Delta a \ \Delta \varepsilon_p}{\varepsilon_c} \qquad (3)$$

where $\Delta\varepsilon_p$ is the plastic strain range experienced over a distance Δa ahead of the crack tip. Extension occurs over Δa when the ΔK-independent critical strain ε_c is achieved. Equation (3) is ΔK-dependent through $\Delta\varepsilon_p$ and Δa, the latter being proportional to the COD within 1 μm of the tip. This model is also consistent with the measured variation in crack tip parameters (Figures 7 and 8) which occurs at any ΔK; thus, it provides a method for bringing together all the crack tip factors which have been measured to date.

The critical strain to fracture model which has been outlined assumes that the crack tip is stationary for a number of cycles until sufficient strain accumulates over Δa. It is also possible to utilize the experimental data in terms of the damage accumulated over the entire plastic zone. Numerical evaluation of these two failure criteria indicates that the critical strain model, which gives a failure strain of about 75%, is more reasonable than the cumulative damage model, which yields a cumulative strain of >212%. The reason for this is thought to be that the cumulative damage model assumes damage to occur equally at both low and high strains (when the product of strain range and number of cycles remains constant); evidently, this is a poor assumption. Examination of the strain distribution indicates that the strain is relatively low within the plastic zone, peaking strongly at the crack tip (Figure 6). This trend increases at higher ΔK. Thus, damage to the material is apparently likewise distributed. The size of the critical element in which strain is accumulating is found to be approximately half the crack tip opening displacement. This small element of material has been referred to as the "process zone" in other theoretical models.

An alternative way of utilizing strains at the crack tip is through the type of expression which has been developed by Weertman[16]

$$\frac{da}{dN} = A \frac{\Delta K^4}{\sigma_y^2 \mu U} \quad (4)$$

where A is a constant, μ is the shear modulus, and stress and strain are combined into an energy term U. We have determined that U decreases with increasing ΔK, which has also been shown to be the case for 2000-series aluminum alloys[17] and for low-carbon steel.[18]

The latter observation was explained in terms of the effects of crack opening mode on the mechanisms of energy dissipation, and based on SEM observations, the same general observations appear relevant to the aluminum alloys. The concepts are shown, schematically, in Figure 9. The range of the present measurements are in the near-threshold region A-B. The ΔK_{TH} is defined as the loading condition when U becomes extremely large, and through Equation (4), $^{da}/dN$ becomes very small. The line ABC represents the decrease in U which would occur if the fatigue crack continued to keep the same mix of Mode I and Mode II as ΔK increased. But at some point, B, the mode mix begins to change, with Mode I becoming much more dominant. At higher ΔK, the value of U may remain constant, as along line BD, or rise, as along line BD'. The latter change was observed in low-carbon steel; exactly what occurs for the aluminum alloys is not clear, but Fine's data[17] indicate some increase (as along BD') may also occur. The point of transition, B, is thought to be determined by the slip characteristics of the material, and such metallurgical factors as grain size, shape, and texture, and perhaps the stress state. For 7075-T6 in the present study, ΔK = 10 $MN/m^{3/2}$ appears to be the beginning of the transition region, because the crack tip strain distribution (mode mix) begins to change at this point.

The techniques developed during the study of crack growth in the ingot alloys have also been used, in a somewhat limited extent so far, to study aluminum alloys derived from advanced powder metallurgy fabrication techniques. Both pre-alloyed X-7091 and mechanically alloyed IN-9051 have been examined.[14] Each alloy exhibited intermittent crack growth behavior. Also, both alloys had larger crack tip opening displacements and crack tip

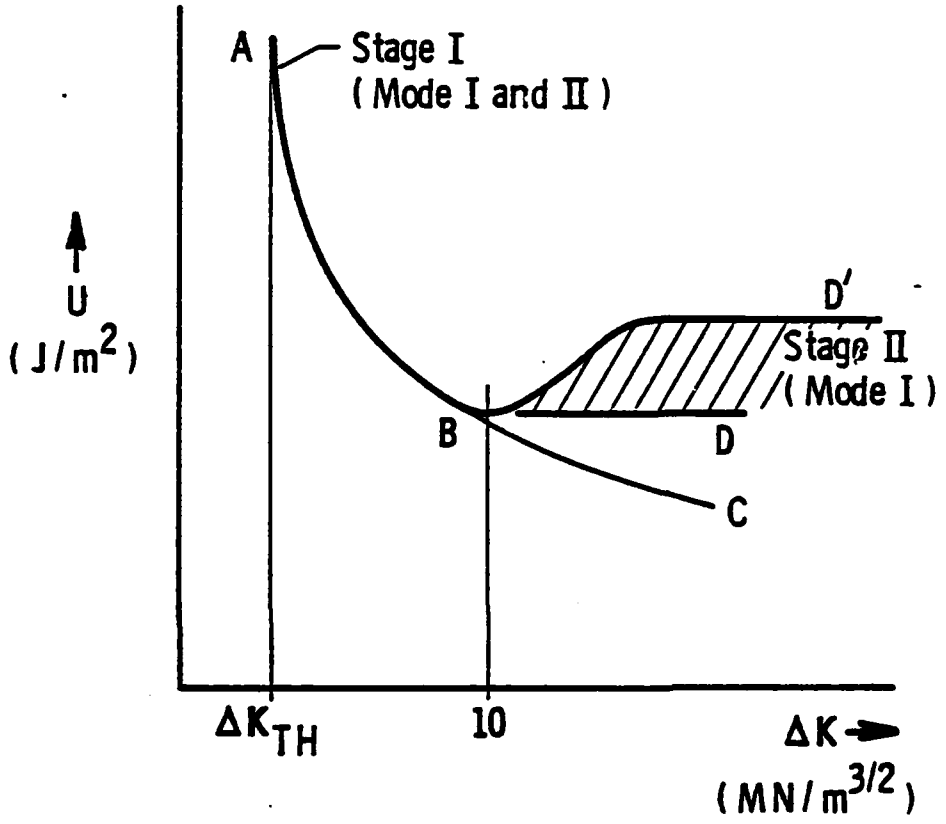

Figure 9. Schematic of the Energy Change with ΔK Showing the Effect of Change in Crack Tip Deformation Mode.

strains than found for the ingot material. These results are still being evaluated in terms of the metallurgical differences between powder metallurgy and ingot alloys.

The stereoimaging technique allows determination of three elements of the normal strain range tensor, and through the use of Mohr's circle, the principal strains and the maximum shear strain. By using the fact that the surface is in plane stress, it is also possible to compute the principal stresses and the maximum shear stress; the method used has been derived from that given by Lubahn and Felgar.[19] The only other information required is an equation relating stress to strain; these relations are empirically derived for the appropriate situation (tension, compression, cyclic). An example of the maximum principal stress field derived from 7075-T6, $\Delta K = 8\ MN/m^{3/2}$, is shown in Figure 10. Similar distributions for minimum principal stress, maximum shear stress, and mean stress are also available from the computations which produced this figure.

Residual stresses developed by a single overload in 7075-T6 have also been calculated from experimental measurements of post-overload deformation fields. This has entailed computing the principal stresses on both the loading and unloading portion of the overload, resolving those stresses back into their normal stress components (x,y), and summing the resulting values. Although the results obtained to date are still being evaluated, the methodology and computational procedure have been developed. An example of the sum of the computed stresses on the next loading half-cycle following a 100% overload is given in Figure 11.

C. Accomplishments

1. The techniques of selected area electron channeling and stereoimaging strain analysis have been developed into useful analytical tools for characterizing fatigue crack tip damage and micromechanics.

2. Fatigue crack tip plastic zone sizes and shapes have been determined, showing deficiencies in current theory,

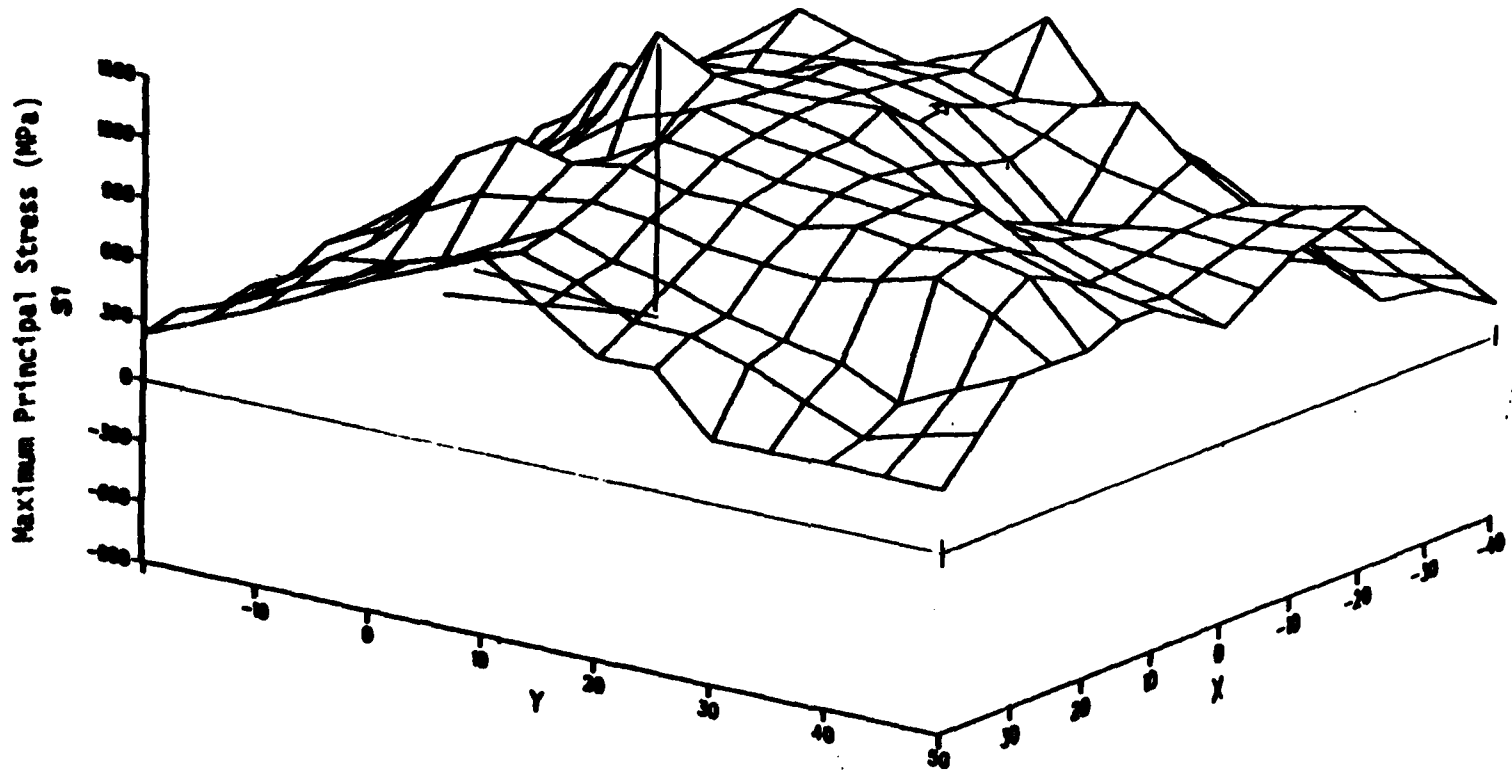

Figure 10. Distribution of Maximum Principal Stress Range, 7075-T6, $\Delta K = 8\ MN/m^{3/2}$; x and y in Micrometers. Crack is shown schematically on plane of zero stress. Load applied along x axis.

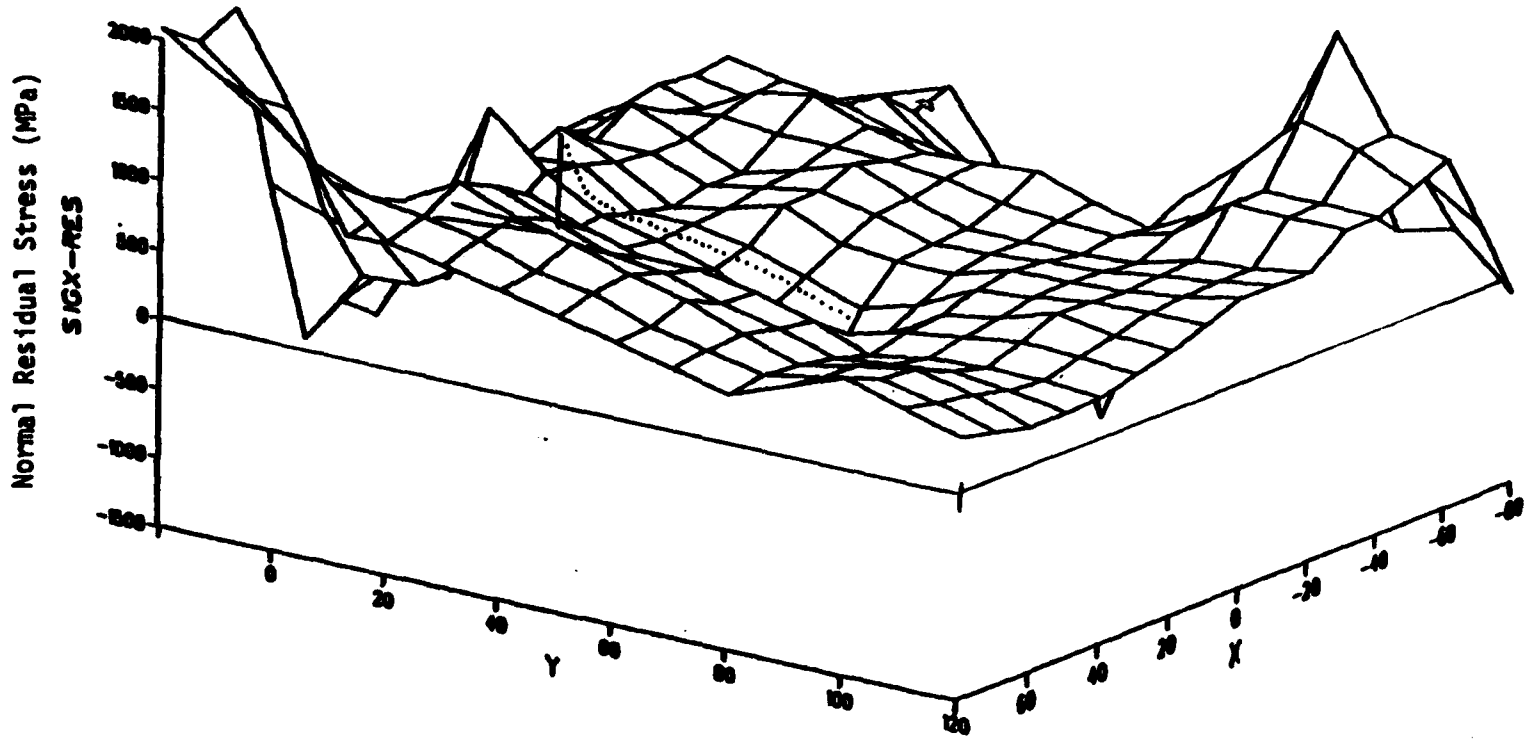

Figure 11. Distribution of the Maximum Stress in the Loading Direction (x) on the Next Loading Cycle After a 100% Single Overload. This represents the sum of the stresses in the x-direction due to the overload cycle plus the stress due to the cycle after the overload. Comparing this to Figure 10 indicates a lack of stress peaking at and ahead of the crack tip. The dotted lines approximate the path of crack growth after the overload cycle.

and having important implications for load spectrum crack growth models in which plastic zone size is a critical input parameter.

3. Use of stereoimaging, and direct observation of crack tips cycled within the SEM, has yielded, for the first time, displacements and strains within as near as 1 μm of the crack tip.

4. Fatigue crack extension has been observed to be discontinuous, and seems to involve the low-cycle failure of a small, local material element on the order of size of the near-tip COD. This process has been quantified, and used successfully in models based on critical strain to fracture and energy to fracture.

5. Local crack tip parameters required for these models, i.e., cyclic strain and COD, have been characterized, and found to depend upon ΔK.

6. Changes in crack tip energy have been correlated with changes in crack opening mode.

7. Crack tip strains have been transformed to crack tip stresses, including the residual stress field following an overload. Progress has been made in using this information to derive the effective crack driving force during post-overload extension.

D. References

1. J. Lankford, D. L. Davidson, and T. S. Cook, Cyclic Stress-Strain and Plastic Deformation Aspects of Fatigue Crack Growth, ASTM STP 637, 1977, p. 36.

2. D. L. Davidson, Proc. Seventh Annual SEM Symposium, 1974, p. 927.

3. D. Broek, Elementary Engineering Fracture Mechanics, Noordhoff International Publishing, The Netherlands, 1974.

4. J. R. Rice and G. F. Rosengren, "Plane Strain Deformation Near a Crack Tip in a Power-Law Hardening Material," J. Mech. Phys. Solids, 16, 1968, 1-12.

5. J. R. Rice, "Mathematical Analysis in the Mechanics of Fracture," in Fracture V. II, ed. by H. Liebowitz, Academic Press, 1968, 191-311.

6. J. Lankford and D. L. Davidson, "Fatigue Crack Tip Plastic Zone Sizes in Aluminum Alloys," International Journal of Fracture, 14, 1978, p. R87.

7. D. L. Davidson and J. Lankford, "Fatigue Crack Tip Plastic Strain in *High Strength Aluminum* Alloys," Fatigue of Engineering Materials and Structures, 3, 1980, p. 289.

8. D. L. Davidson, "Fatigue Crack Tip Displacement Observations," Journal of Materials Science, 14, 1979, p. 231.

9. D. L. Davidson and J. Lankford, "Dynamic, Real-Time Fatigue Crack Propagation at High Resolution as Observed in the Scanning Electron Microscope," Fatigue Mechanisms, ASTM STP 675, American Society for Testing and Materials, 1979, p. 277.

10. D. L. Davidson, "The Observation and Measurement of Displacements and Strain by Stereoimaging," SEM/1979, 1979, pp. 79-86.

11. D. R. Williams, D. L. Davidson, and J. Lankford, "Fatigue Crack Tip Plastic Strains by the Stereoimaging Technique," Experimental Mechanics, 20, 1980, p. 134.

12. D. L. Davidson, "A New Method for Measuring Crack Tip Strains," Inst. of Physics Conf. Series 52 (EMAG'79), Inst. of Physics, London, 1980, pp. 21-24.

13. D. L. Davidson, "Fatigue Crack Plasticity: Dynamic and Static Observations," SESA Annual Conf. Proceedings, pp. 187-189, 1981.

14. D. L. Davidson and J. Lankford, "Fatigue Crack Tip Plasticity and Crack Growth Mechanics in Powder Metallurgy and Wrought Aluminum Alloys," Proceedings of: High Performance Aluminum Powder Metallurgy Alloys, TMS-AIME, 1982 (in press).

15. D. L. Davidson and J. Lankford, "Fatigue Crack Tip Strains in 7075-T6 by Stereoimaging and Their Use in Crack Growth Models," Quantitative Measurement of Fatigue Damage, ASTM STP 811, 1983 (in press).

16. J. Weertman, Inter. J. Fracture, V. 9, 1973, pp. 125-131.

17. P. K. Liaw, S. I. Kwan, and M. E. Fine, Metallurgical Trans. A, V. 12A, 1981, pp. 49-55.

18. D. L. Davidson, Fatigue of Engineering Materials and Structures, V. 3, 1981, pp. 229-236.

19. J. D. Lubahn and R. P. Felgar, Plasticity and Creep of Metals, John Wiley and Sons, Inc., New York, 1961, pp. 321-325.

II. TITANIUM ALLOY TASK

J. E. Hack and G. R. Leverant

A. Research Objectives

1. Determine the mechanism which controls the reduction of fatigue life found in beta-annealed titanium alloys during dwell fatigue cycling.
2. Determine the key microstructural features in the mechanism.
3. Predict the relative susceptibility of titanium alloys in general to dwell fatigue as a function of microstructure.
4. Determine the feasibility of creating a dual microstructure with a fatigue crack initiation resistant surface layer and fatigue crack growth resistant core by a thermal-mechanical treatment which would be adaptable to current fabrication procedures.

B. Summary of Research Efforts

1. The Role of Microstructure in the Susceptibility of Titanium Alloys to the Effects of Dwell Times at Peak Load.

Five commercial titanium alloys were examined in this study. These included three near-alpha alloys: Ti-6Al-5Zr-0.5Mo-0.25Si (IMI-685), Ti-5Al-2.5Sn (5-2.5), and Ti-5.5Al-3.5Sn-3Zr-0.25Mo-0.35Si (IMI-829); and two alpha-beta alloys: Ti-6Al-4V (6-4) and Ti-6Al-2Sn-4Zr-2Mo-0.1Si (6-2-4-2). All materials were processed to give a large colony structure with a colony size of 400 to 750 μm. The microstructure and processing conditions for each alloy are given in Figure 1. Complete chemical analyses and summaries of tensile properties are presented in Tables I and II.

a)

b)

Figure 1. Microstructures and Processing Conditions of the 5 Alloys Studied. (a) IMI-685 - cut from a forging which had been beta blocked, alpha + beta finished, followed by a beta anneal @ 1323 K, oil quenched, and stress relieved @ 1123 K. (b) Ti-5Al-2.5Sn - cut from bar stock and subsequently beta annealed @ 1338 K for 2 h, furnace cooled, and aged @ 863 K for 8 h.

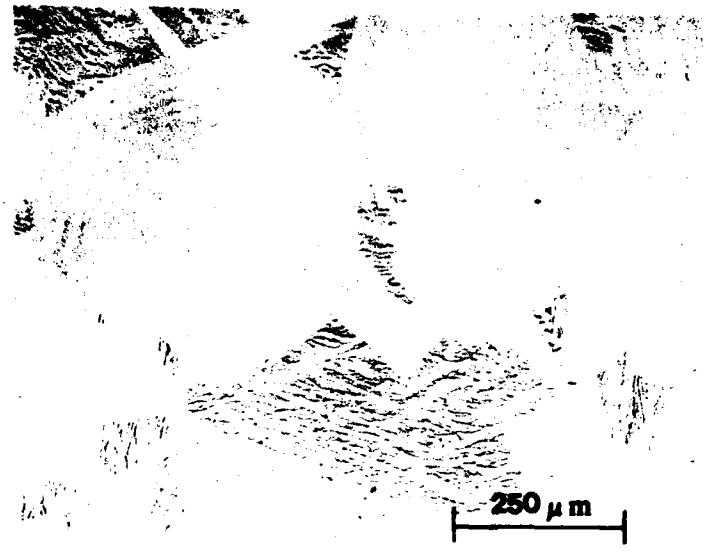

c)

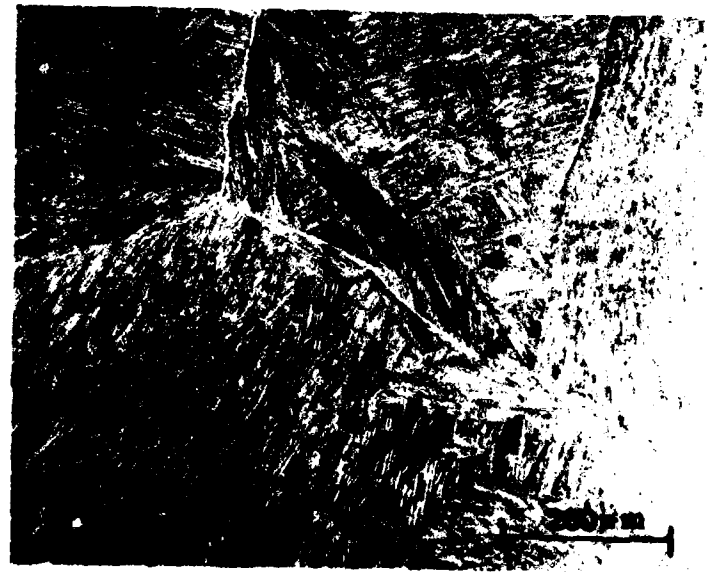

d)

Figure 1 (Continued). Microstructures and Processing Conditions of the 5 Alloys Studied. (c) IMI-829 - cut from a forging which had been beta blocked, alpha + beta finished, followed by a beta anneal @ 1323 K, oil quenched, and aged @ 898 K for 2 h. (d) Ti-6Al-2Mo-4Zr-2Sn + 0.1Si - cut from bar stock and subsequently beta annealed @ 1338 K for 2 h, furnace cooled and aged @ 863 K for 8 h.

e)

Figure 1 (Continued). Microstructures and Processing Conditions of the 5 Alloys Studied. (e) Ti-6Al-4V - cut from a forging and subsequently beta annealed @ 1338 K for 2 h, furnace cooled, and aged @ 863 K for 2 h.

TABLE I

ANALYZED COMPOSITIONS FOR MATERIALS STUDIED

Alloy	Composition (Wt. Percent)							Composition (ppm)		
	Al	Sn	Zr	Mo	Nb	V	Si	O	N	H
IMI-685	5.2	-	5.3	0.44	-	-	0.27	1200	10	40
Ti-5Al-2.5Sn	5.3	2.6	-	-	-	-	-	1750	230	90
IMI-829*	5.5	3.5	3.0	0.25	1.0	-	0.35	-	-	32
Ti-6Al-2Sn-4Zr-2Mo + 0.1Si	5.1	1.9	5.2	1.9	-	-	0.09	1400	12	90
Ti-6Al-4V	6.3	-	-	-	-	4.3	-	1750	140	60

*Wt. percent values are nominal, not analyzed; ppm value of H is a measured value.

TABLE II

PERTINENT TENSILE PROPERTIES OF THE MATERIALS STUDIED

Alloy	Yield Strength (MPa)	Plastic Strain To Failure (pct)
IMI-685	876	6.9
Ti-5Al-2.5Sn	855	8.5
IMI-829	876	10.1
Ti-6Al-2Sn-4Zr-2Mo + 0.1Si	862	5.5
Ti-6Al-4V	883	10.5

The most extensive testing was performed on IMI-685. Samples of IMI-685 were tested at room temperature in displacement-controlled cantilever bend fatigue, load-controlled axial fatigue, and static axial loading conditions. Specimen geometries for the bending and axial tests are shown in Figure 2. Displacement and load-controlled fatigue testing were performed by both continuous cycling and with a five-minute dwell time at peak load, hereafter referred to as dwell fatigue. Axial dwell fatigue tests were also run on IMI-685 at 473 K and 203 K. The peak load applied to the 473 K specimen was 95 pct of the yield stress at 473 K or 610 MPa. In addition, a load-controlled axial dwell fatigue test was performed on IMI-685 material which had been charged with hydrogen to a bulk level of 140 ppm, as compared to the as-received level of 40 ppm. Charging was performed in a modified Sievert's apparatus. A series of sustained-load experiments on IMI-685 was halted at various percentages of expected lifetime and the specimens were metallographically sectioned to allow inspection for internal cracking. An acoustic emission transducer was placed on the specimens during the experiments and the results of the output were correlated with the extent of internal cracking.

Testing of the remaining four alloys was confined to load-controlled axial fatigue under continuous and dwell cycling and static load conditions at room temperature. Smooth specimens were used in all cases. A maximum stress of at least 95 pct of the yield stress was applied to ensure the activation of creep processes during hold times. Creep strains were measured by a clip gage where appropriate. An R ratio of 0.3 was used in all fatigue tests except where noted.

Microstructural characterization and fractographic analysis were performed by optical and scanning electron microscopy. In addition, two-stage replicas of the alloy microstructures were produced and examined by transmission electron microscopy.

Table III shows a comparison of fatigue life of IMI-685 as a function of cyclic waveform and load vs displacement control. As can be seen from the data, the presence of a five-minute dwell at peak load in the fatigue cycle drastically reduced lifetime compared to a triangular waveform, twenty

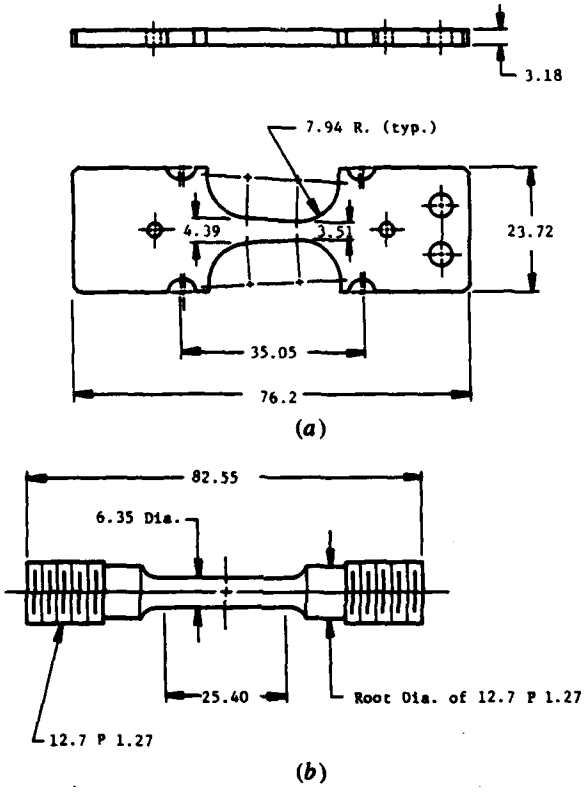

Figure 2. Cantilever Bend and Axial Fatigue Test Specimen Geometries (all dimensions are in mm). (a) Cantilever bend specimen. (b) Axial specimen.

TABLE III

COMPARISON OF AXIAL AND BENDING FATIGUE RESULTS ON IMI-685

Loading	R-Ratio	Dwell Period (Minutes)	Cycles to Failure	Source
Axial	0.3	0	37,958 29,845 34,215 39,523	Reference 1
Axial	0.3	5	790 217	Reference 1
Axial	0.3	5	173	This study
Bending	0.05	0	27,713 33,280	This study
Bending	0.05	5	7,163* 16,491	This study

*Initial 4906 cycles at R = 0.05; remaining cycles at R = 0.3.

cpm test. Also, although the twenty cpm specimens had the same lifetimes in axial and bend tests, the dwell lives were significantly longer in bending.

Axial tests were conducted on IMI-685 specimens with a five-minute dwell at peak stress; a five-minute dwell at peak stress combined with a five-minute dwell at minimum stress; a 1 pct plastic prestrain followed by cycling with a five-minute dwell at peak stress; and under static stress conditions equivalent to the peak stress level. In all instances, the peak stress was 830 MPa or 95 pct of the 0.2 pct offset yield strength.

The results for these tests are given in Figure 3. The figure shows that cyclic loading with a five-minute dwell at peak stress or static loading only resulted in identical times and strains to failure. The specimen that was prestrained in tension failed in a much shorter time at load in subsequent dwell cycling but at the same overall strain to failure as the dwell fatigue and statically loaded specimens. The specimen cycled with a five-minute dwell period at both the minimum and maximum loads also failed at the same strain level but in a much longer time at load.

Table IV shows a comparison of the results of dwell fatigue tests on IMI-685 in the as-received condition at 473 K and 203 K and in the hydrogen charged condition at room temperature with previous results for similar tests on as-received IMI-685 at room temperature. The results show a lack of dwell effect (either in lifetime or ductility) at both elevated and cryogenic temperatures in the as-received material. However, an increase in hydrogen content at room temperature dramatically reduced lifetime by an additional factor of 30 in comparison with the reduction already found in as-received material.

The results of interrupted sustained-load tests on smooth specimens of IMI-685 run at 95 pct of the 0.2 offset yield stress and room temperature are presented in Table V. Specimen 2 was the only sample in which acoustic emission events above background levels were detected.* The acoustic

*The resonant type transducer used allowed only the detection of large amplitude events above background and not the characterization of an event signature.

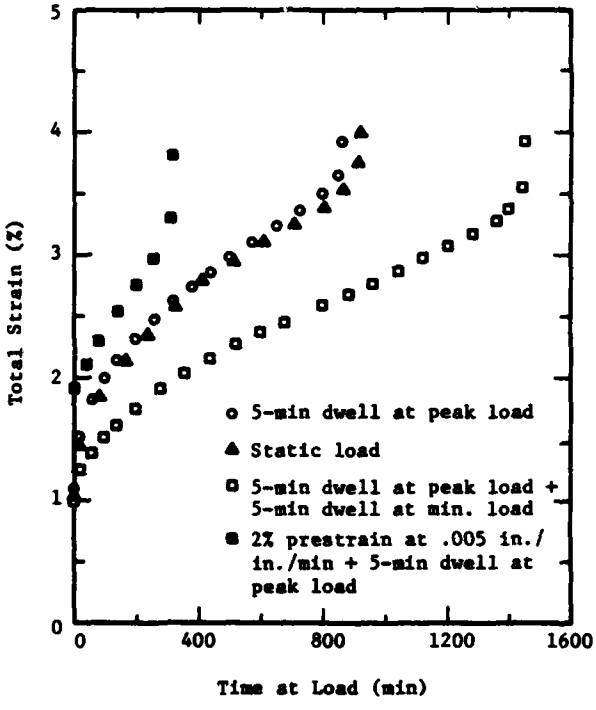

Figure 3. Results of Room Temperature Load-Controlled Axial Dwell Fatigue Tests on IMI-685.

TABLE IV

EFFECTS OF TEST TEMPERATURE AND HYDROGEN CONTENT ON DWELL FATIGUE BEHAVIOR OF IMI-685

Hydrogen Content (ppm)	Test Temperature (K)	Cycles to Failure	Plastic Strain to Failure (pct)
40	298	173	3.2
40	203	>1665*	0.0**
40	473	834	17.0
140	298	6	3.3

*Specimen did not fail.
**No creep occurred.

TABLE V

RESULTS OF INTERRUPTED SUSTAINED-LOAD TESTS ON IMI-685

Minutes at Peak Load	Total Plastic Strain (pct)	Number of Acoustic Emission Events Detected	Number of Areas Cracking Found
200	0.84	0	0
400	1.75	3	3
600	0.90	0	0

emission events occurred at 0.8 pct, 1.1 pct, and 1.6 pct plastic strain. As indicated in Table V, there appeared to be a correlation between the occurrence of acoustic emission events and internal cracking.

Table VI shows a comparison of results of tensile, dwell fatigue, and sustained-load tests for IMI-685 and the other four alloys studied. As can be seen from the data, the 5-2.5 alloy shows a reduction in lifetime in dwell fatigue as compared to 20 cpm cycling, similar to IMI-685. In addition, when held at maximum load during testing, the three near-alpha alloys all demonstrate a drastic reduction in strain to failure compared to that found in a tensile test. The 6-2-4-2 and 6-4 alloys do show shorter lifetimes in dwell tests run at or near their respective yield stresses, but no loss in ductility as compared to a tensile test. In fact, the dwell fatigue and static load samples of 6-2-4-2 and 6-4 all had strains to failure slightly in excess of those measured in tensile tests.

Fractographic examination of the samples used for the tests summarized in Figure 3 revealed similar features for all the test conditions.[2] Each fracture surface had at least one subsurface area, one to two colony diameters in extent, which had a cleavage-like appearance and was inclined at a significant angle to the plane of maximum normal stress. An example of such a facet is shown in Figure 4. No apparent defects were visible at the initiation sites of these subsurface cleavage facets.

As described previously, the reduction in lifetime associated with dwell fatigue of the hydrogen charged IMI-685 specimen was an order of magnitude greater than that which occurred in as-received material. Examination of the fracture surface of the charged specimen revealed almost complete brittle behavior. This is shown clearly in Figure 5. The fracture surface of the IMI-685 dwell fatigue specimen run at 473 K showed no indication of brittle failure.

The samples of IMI-685 which were interrupted at various times under load were subsequently sectioned and polished through to determine the occurrence and extent of internal cracking. Cracking was found only in specimen 2 (see Table V). Three distinct areas of cracking were found in this specimen. This correlates well with the number of detected acoustic

Figure 4. Typical Subsurface Cleavage Facet on the Fracture Surface of a Dwell Fatigue Specimen of IMI-685.

Figure 5. Brittle Failure in a Dwell Fatigue Specimen of IMI-685 Containing 140 ppm Hydrogen.

emission events. A typical area is shown in Figure 6. In all three areas, several parallel cracks were found grouped together within a single colony.

Figure 7 shows cleavage facets typical of dwell fatigue and sustained-load specimens in the 5-2.5 and IMI-829 alloys. The facets are similar in nature to those found in samples of IMI-685. No brittle facets were found on dwell and sustained-load specimens of the 6-2-4-2 and 6-4 alloys. Some areas which appeared relatively flat under macroscopic observation were determined to be the result of ductile failure upon examination at higher magnification (Figure 8).

The mechanical test and fractographic results on IMI-685 samples reveal two significant aspects of the embrittlement process in this alloy. First, the results in Table III and Figure 3 indicate a critical dependence on the buildup of time-dependent plastic strain. Titanium alloys have been shown to exhibit substantial creep deformation when loaded above 90 pct of their yield stress at room temperature.[3,4] Apparently this creep led to stress relaxation in the displacement-controlled dwell tests which increased the lives compared to the load-controlled dwell tests where stress relaxation was not possible. The fact that time (at load) to failure and failure mode were identical for specimens which underwent dwell fatigue or static loading indicates that fatigue cracking actually plays an insignificant role in the failure process at the stress level studied. In addition, the sample that was prestrained in tension failed in a much shorter time at load in subsequent dwell fatigue but at the same overall strain to failure and with the same fracture features as the dwell and static loaded specimens. Also, specimen 2 in the interrupted static load tests was the only specimen which showed evidence of internal cracking and was also the only sample of those tested which crept at a sufficiently high rate to develop a significant amount of plastic strain during the test period.

All of these results indicate that strain accumulation to a critical level is an important component of the failure mode. However, the extended lifetime of the specimen with a five-minute dwell period at maximum and minimum load indicates that creep strain is not the only time dependent phenomenon which takes part in the failure process as complete recovery of

Figure 6. Subsurface Cleavage Cracking in a Specimen of IMI-685 Which was Held at Load for 400 Min and Subsequently Sectioned.

Figure 7. Typical Subsurface Cleavage Facet on Dwell Fatigue and Sustained-Load Specimens of Ti-5Al-2.5Sn.

Figure 8. High Magnification SEM Fractograph of a Macroscopic Facet on the Sustained-Load Specimen of Ti-6Al-2Mo-4Zr-2Sn + 0.1Si Showing Ductile Tearing of the Beta Phase.

creep strain would not be expected in the time period at lower stress. This observation is consistent with that of Evans and Gostelow.[5]

Electron channeling patterns of facets similar to those found on the dwell fatigue and static load IMI-685 specimens revealed that they generally corresponded to a basal or near-basal plane.[6] The occurrence of this type of cleavage-like fracture in precracked sustained-load cracking specimens has usually been associated with hydrogen embrittlement processes.[7,8] The presence of the near-basal plane facets strongly implies that internal hydrogen as well as time dependent deformation is important to the fracture process.

This point is more clearly illustrated in the results shown in Table IV. 473 K represents a regime where creep processes can readily occur but titanium hydrides are thermodynamically unstable,[9] while at 203 K hydride formation is strongly favored[10] but creep did not occur during the test. In neither case did embrittlement occur. (It should be noted that the 203 K test was run out to an order of magnitude longer time than the test at room temperature to allow for slower diffusion of hydrogen at this temperature.) An increase in hydrogen content at room temperature, where both creep deformation and hydride precipitation may be active, led to a dramatic reduction in the time required for embrittlement to occur. Thus, both the time-dependent deformation and internal hydrogen play a significant role in the failure process, but neither is sufficient to induce embrittlement when acting alone.

It is obvious from the above discussion that time-dependent deformation and the presence of hydrogen are both critical to the formation of subsurface cleavage facets that are associated with the embrittlement of IMI-685. Several models have been proposed for subsurface cleavage crack initiation in titanium alloys based on strictly time-independent mechanical processes such as dislocation reactions produced during deformation.[11,12,13] However, none of these models addresses the contribution of internal hydrogen to the failure process. A model which incorporates both creep strain and internal hydrogen has been developed[14] to explain the embrittlement of IMI-685. The model ties these two factors together through the substantial hydrostatic

stresses present at or near the tip of a stressed planar shear band. A brief development of the model is given below.

Since the cleavage facets associated with embrittlement are coincident with or at a low angle to the basal plane, which is a prominent slip plane in titanium alloys with a moderate to high aluminum content,[15] it was appropriate to investigate the role of a shear band in the fracture process. One way in which a shear band can locally concentrate hydrogen is by the creation of a hydrostatic stress field at the tip of a blocked pileup of dislocations. Such a stress field would attract an increased hydrogen concentration by diffusion.[16] Since strain-induced hydride formation has been observed in thin foils of IMI-685 near the tip of a crack,[17] this mechanism was considered further.

All materials in which the dwell effect was observed had large colonies (400 to 750 μm) with very planar slip characteristics. In such a microstructure, a shear band can extend across a subsurface colony and be blocked at the colony boundaries. This situation creates a stressed, double-ended dislocation pileup. For the purposes of the model, such a band is considered to consist of a single planar array of edge dislocations as shown in Figure 9. This geometry has long been recognized as analogous to a shear or Mode II crack.[18]

The hydrostatic stress field due to the shear band can then be calculated from expressions for the stresses around a Mode II crack and compared with the equivalent Mode I-Mode II crack which would be formed by cleavage along the shear band. A plot of the results of such a calculation is given in Figure 10. As can be seen from the figure, the hydrostatic tensile stress due to the shear band is a maximum along the bottom surface of the band and directly behind the blocked tip of the band. The top of the band actually has compressive hydrostatic stresses present. Also, a significant fraction of the maximum level of hydrostatic stress is maintained within about 20 deg of the orientation of the maximum value. The most striking feature of the figure is that the magnitude of the maximum hydrostatic tensile stress attendant to the shear band is within a factor

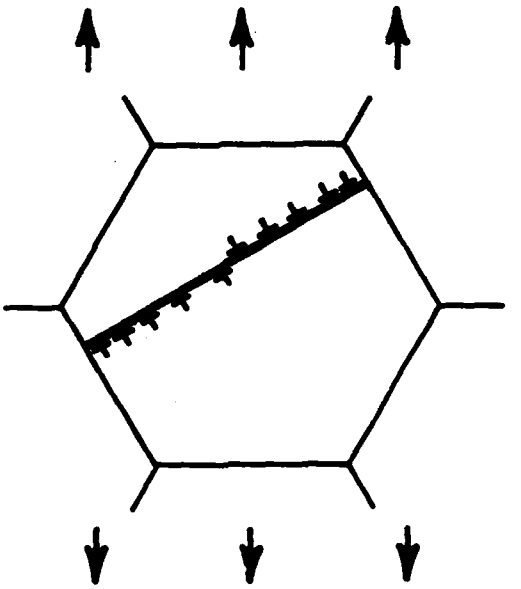

Figure 9. Schematic of Double-Ended Dislocation Pileup Blocked at Both Ends by a Colony Boundary.

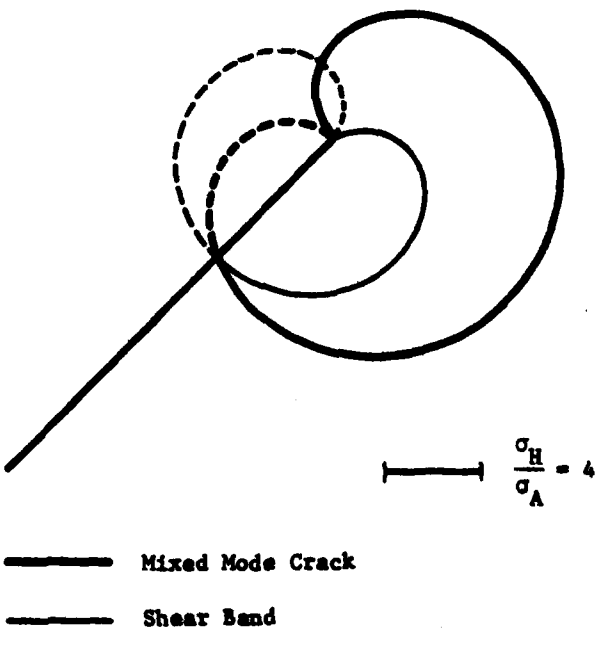

Figure 10. Calculated Distribution of Hydrostatic Stress/Applied Stress (σ_H/σ_A) 1 μm from the Tip of an Equivalent Shear Band and Mixed Mode I-Mode II Crack at 45 Deg to the Tensile Axis. Dashed lines indicate hydrostatic compression, while solid lines indicate hydrostatic tension.

of 1.4 of the maximum hydrostatic tensile stress due to the mixed-mode crack when the two values are normalized to the same applied stress.

In addition, metallographic observations on axial dwell test specimens of IMI-685 showed that, in numerous instances, secondary cracks were present which only partially traversed a single large Widmanstatten colony.[2] Thus, the cracks formed along shear bands do not necessarily cleave the entire shear band at once. Since some of the cracks can grow and lead to complete failure, the half-crack length assumed for the mixed-mode crack in the calculations may be too large. Most likely the proposed mechanism would initiate a small microcrack in the hydrogen-rich region near the blocked tip of the shear band which would then propagate by the repeated formation and cracking of hydrides at the crack tip. Taking this into account, the hydrostatic tensile stresses due to the shear band can easily attain comparable levels to those for a growing crack which are large enough to cause hydrogen diffusion to the tip of the band. Although microvoid initiation at the intersection of a slip band and a grain boundary in titanium by purely mechanical means has been observed,[19] it is likely that an increased local concentration of hydrogen would reduce the energy required for void or microcrack initiation to occur.

Such a model is consistent with the results obtained on all three of the near-alpha alloys tested in this study. A five-minute dwell at minimum load would be expected to relax the stress at the tip of a blocked shear band. This allows hydrogen to diffuse down any accumulated concentration gradient and extend the lifetime of the specimen, as observed in Figure 3. Also, if no creep deformation were to occur, as in the dwell test performed at 203 K, no stress concentrator would be established and no driving force for a localized accumulation of hydrogen would exist. Thus, the hydrogen embrittlement phenomenon would not be expected to take place. In addition, microstructural features associated with the dwell debit coincide with predictions based on the model. A cleavage facet on the surface of an IMI-685 dwell specimen was sectioned through its initiation site and carefully polished down to reveal the microstructure at the facet origin. This technique was successfully used by Kerr et al to determine defects at

fracture initiation sites in powder metallurgy titanium compacts.[20] The only significant microstructural characteristic present in the region of the cleavage initiation site was a colony boundary. The model predicts that initiation should take place at colony boundaries where slip is blocked.

This is graphically displayed in Figure 11 which shows a cross section of the IMI-685 held at maximum load for 400 minutes. In this photograph, it can be seen that the two parallel cracks extend from a colony boundary across the colony. One is quite long and extends nearly across the entire colony while the other has not propagated very far from the boundary. Close examination of the regions slightly above the cracks shows slip bands which traverse across the grain and impinge on the colony boundary at precisely the point at which the cracks intercept the boundary. The information in Figure 11 strongly supports the hypothesis that initiation of the facets occurs at the intersection of shear bands and colony boundaries.

The model described in the previous section is not limited in applicability to IMI-685. Similar embrittlement would be predicted in any titanium alloy with the large colony microstructure where long shear bands, thus high hydrostatic stress levels capable of driving hydrogen diffusion, may be generated. However, the results presented in Table VI show that while the other two near-alpha alloys, 5-2.5 and IMI-829, were susceptible to embrittlement during dwell or sustained-load conditions, the two alpha-beta alloys, 6-4 and 6-2-4-2, were not. Thus, the fact that large grains and long shear bands were present appeared to be necessary but not sufficient conditions to induce cleavage fracture in the alloys studied.

This apparent inconsistency was resolved by a closer examination of the microstructure in the five alloys. Figure 12 shows a comparison of the IMI-685 and 6-2-4-2 structures. As can be seen from the figures, the near-alpha IMI-685 consists of very fine alpha platelets bounded by discontinuous beta phase. A similar distribution of beta phase was found in the other two near-alpha alloys. The 6-2-4-2 structure, on the other hand, is coarser, and the beta phase is thicker and more continuous. This is consistent with

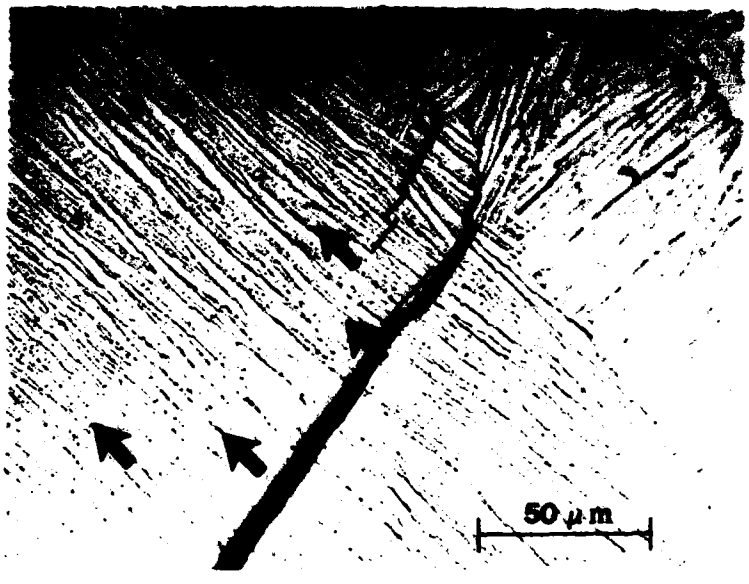

Figure 11. Subsurface Cleavage Cracking in a Specimen of IMI-685 Which was Held at Load for 400 Min and Subsequently Sectioned. Note the initiation of cracking at slip-band colony boundary intersections. The slip band is denoted by arrows.

TABLE VI

SUMMARY OF RESULTS OF LOAD-CONTROLLED, AXIAL DWELL, AND SUSTAINED-LOAD TESTS ON ALL ALLOYS STUDIED

Alloy	Type of Loading	Maximum Load (pct Yield Strength)	Cycles to Failure	Plastic Strain to Failure (pct)
IMI-685	Static load	95	-	3.1
	5-min. dwell at peak load	95	173	3.2
	20 cpm	95	>30,000	-
	Tensile test	-	-	6.9
Ti-5Al-2.5Sn	Static load	95	-	3.7
	5-min. dwell at peak load	95	103	4.4
	20 cpm	95	12,303	-
	Tensile test	-	-	8.5
IMI-829	Static load	95	-	2.1
	5-min. dwell at peak load	95	369	2.0
	Tensile test	-	-	10.1
Ti-6Al-2Sn-4Zr-2Mo + 0.1Si	Static load	95	-	6.9
	5-min. dwell at peak load	100	178	6.4
	Tensile test	-	-	5.5
Ti-6Al-4V	5-min. dwell at peak load	95	512	11.5
	Tensile test	-	-	10.5

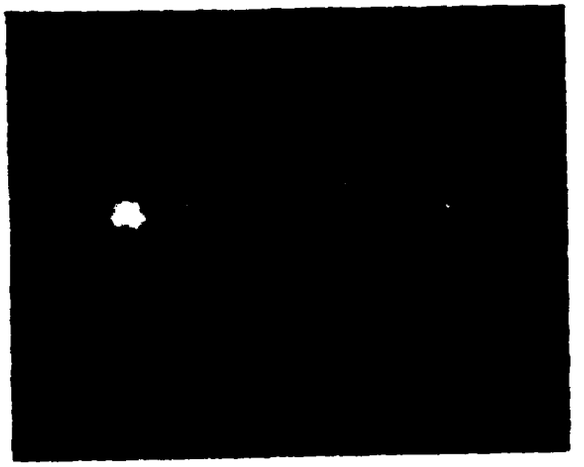

a)

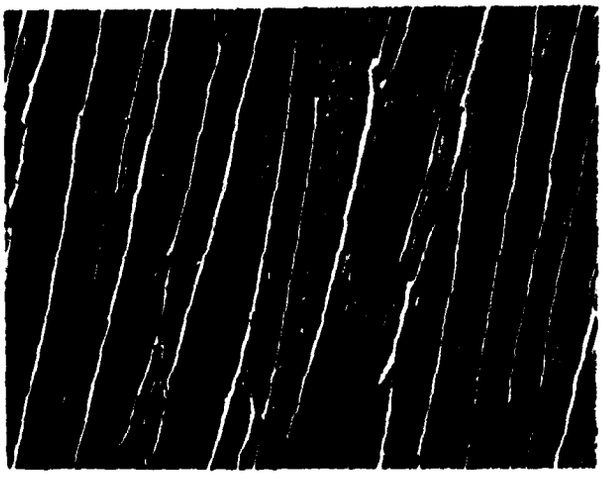

b)

Figure 12. TEM Micrographs of 2-Stage Replicas of Typical Near-Alpha and Alpha-Beta Alloy Microstructures. (a) IMI-685. (b) Ti-6Al-2Mo-4Zr-2Sn + 0.1Si.

the beta phase distribution in the 6-4 alloy. It has long been known that the solubility of hydrogen in beta titanium is over an order of magnitude higher than that for the alpha phase.[21,22] Also, the beta phase can apparently tolerate hydrogen levels close to its solubility limit without a significant loss in ductility or the onset of stress-induced hydride formation.[21] Although a thick continuous layer of beta phase which surrounds an alpha platelet does not present a crystallographic barrier to the shear band, it can act as a crack blunter if the alpha were to cleave. However, if the beta film is very fine or discontinuous, it will not present an effective barrier to cleavage and, indeed, the crack may be able to follow a path which lies almost entirely in the alpha phase. A schematic depicting this situation is shown in Figure 13. These processes are similar to those described by Nelson[23] in his comparison of stress corrosion cracking and external hydrogen embrittlement in titanium alloys. Such behavior is consistent with the observed cleavage facets observed in the near-alpha alloys (Figure 4) and the evidence of alternating alpha cleavage and ductile rupture at beta plates in the alpha-beta alloys (Figure 8).

Additional work was performed on the 5-2.5 alloy which was beta-annealed at 1338 K for 2 hours in vacuum and furnace cooled. The material was then re-annealed at 1325 K for 1 hour in argon and furnace cooled. This resulted in a microstructure similar to those in Figure 1b but on a much coarser scale. Several specimens were charged with hydrogen to various levels in a modified Sievert's apparatus.

The results of sustained-load tests on these specimens are presented in Table VII.

The data clearly shows a competition between ductile failure, due to the low creep resistance associated with the coarse microstructure, and brittle behavior due to hydrogen embrittlement. The creep strain is required to establish the shear bands that act, in turn, as stress concentrators. However, if the creep rate is high enough, failure occurs by creep before the hydrogen has enough time to diffuse to the tips of the shear bands. In general, then, at lower hydrogen contents and high loads,

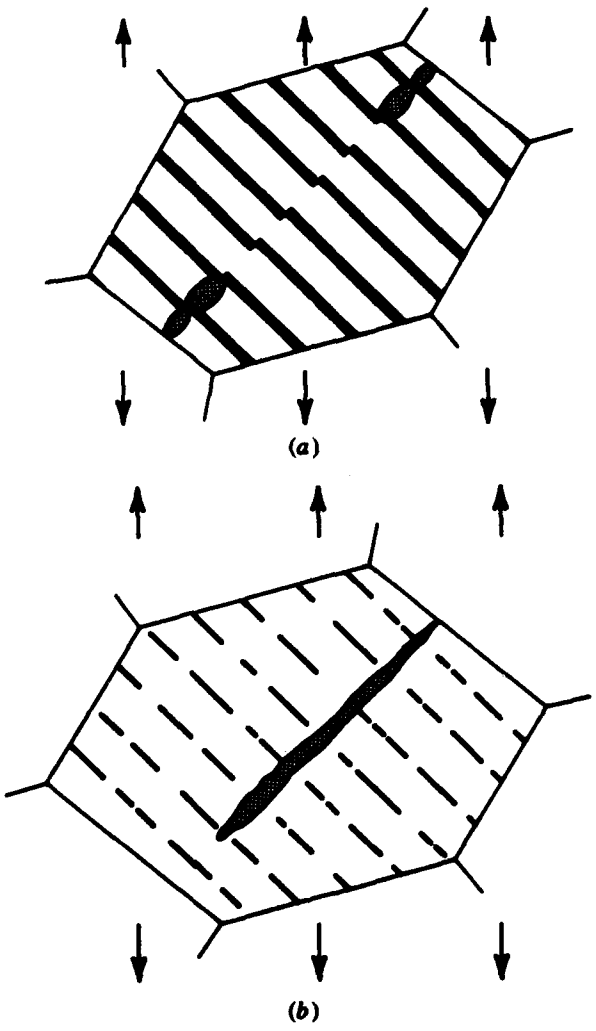

Figure 13. Schematic of Hydrogen-Assisted Crack Behavior in Large Colony Material. (a) Crack blunted by thick, continuous beta phase. (b) Crack able to propagate in embrittled alpha phase.

TABLE VII

SUMMARY OF RESULTS OF SUSTAINED-LOAD
TESTS ON HYDROGEN-CHARGED Ti-5Al-2.5Sn

H_2 Content (ppm)	Yield Strength Percent	Total Strain to Failure	Time to Failure (min)
100	90	6.3	92
150	80	3.7	1680
150	85	4.9	87
200	80	3.8	464
200	85	4.9	206
250	85	1.5	10
250	75	1.5	547
350	80	2.2	6

*The tensile elongation of the 100 ppm specimen was 5% and the 0.2% offset yield strength was 876 MPa.

a short failure time is observed but the total elongation is on a par with that found in a tensile test. As the hydrogen content is increased, and/or the load is reduced (but still high enough to cause a stable creep rate), the percentage brittle failure increased. At hydrogen contents above 200 ppm, smooth steps, as in Figure 5, formed across the specimen and the total elongation to failure decreased drastically. Usually such large reductions are not reflected in the tensile properties.

2. Dual Microstructure Titanium Alloys

Ti-6Al-4V (beta annealed at 1338 K for 2 hr., furnace cooled, and aged at 863 K for 2 hr.) was used for the experiments. The microstructure was identical to that shown in Figure 1e. Cold work was introduced into the surface of test coupons by shot peening to an intensity of .010-.011 on the Almen C scale. This very high intensity was selected to ensure that the cold work penetrated to a significant depth. After peening, the coupons were annealed for one hour at either 1116 K or 1144 K in either argon or vacuum.

At both temperatures, a zone of fine recrystallized grains was formed at the surface. This microstructure extended up to a depth of approximately 50 μm but was very non-uniform and even absent in some locations, Figure 14a. The depth was greatest at the corners of the coupons, Figure 14a, apparently due to the increased degree of cold work experienced at these locations.

Small surface flaws were also found in some locations, Figure 14b. These are a consequence of the very high peening intensity that was intentionally selected to maximize the degree of cold work.

This small study has demonstrated the feasibility of producing a dual microstructure that might be highly resistant to fatigue cracking. Clearly, considerable additional work would be needed to optimize such an approach.

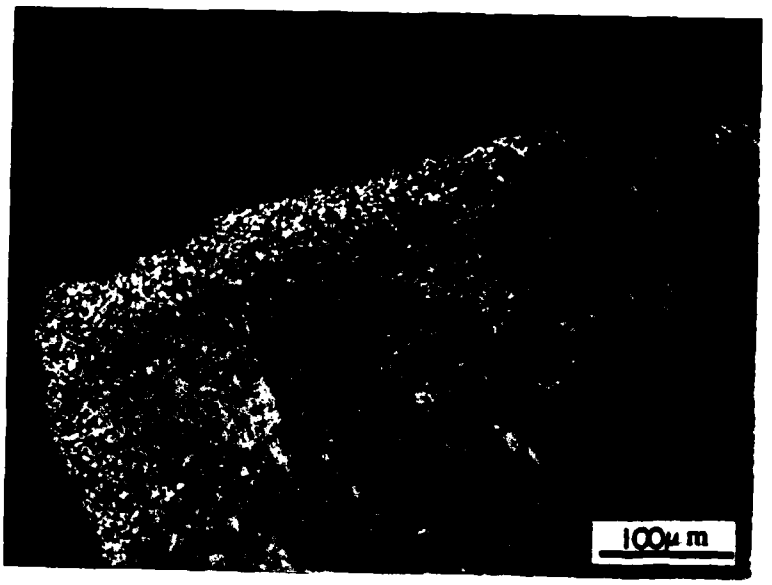

a)

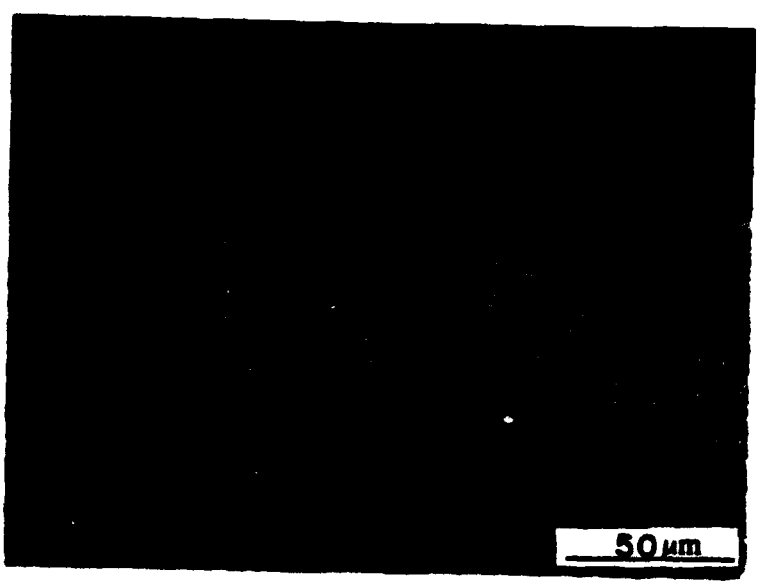

b)

Figure 14. Near-Surface Microstructure, Beta-Annealed Ti-6Al-4V. (a) Surface zone of fine recrystallized grains; (b) surface flaws caused by peening.

C. Accomplishments

1. The large reductions in fatigue life in IMI-685 during dwell cycling observed in this and other studies were found to be due to an internal hydrogen embrittlement phenomenon and not a creep-fatigue interaction.

2. Both time-dependent deformation and internal hydrogen were shown to be required for embrittlement to occur with the blocked shear bands accompanying creep strain providing the source of hydrostatic tension that leads to localized increases in hydrogen content and subsequent embrittlement.

3. The key microstructural features controlling the embrittlement process have been determined to be a large transformed beta colony size and the morphology and distribution of the beta phase at the alpha interplatelet boundaries. Colony size is important because the maximum level of hydrostatic tensile stress obtainable is proportional to the length of a blocked shear band, which is equivalent to the colony diameter. Fine, discontinuous films of beta phase at the alpha phase interplatelet boundaries allow easy fracture through hydrogen embrittled alpha, while thick, continuous plates of beta act as a ductile, crack blunting phase.

4. The relatively small amount of retained beta phase in near-alpha titanium alloys leads to fine, discontinuous beta distributions in this class of alloys. Their inherent susceptibility to internal hydrogen embrittlement under sustained-load conditions must be taken into account whenever beta-processed, near-alpha titanium alloys are considered for structural applications below ~400°F.

5. A possible thermal-mechanical approach to the achievement of dual microstructure titanium alloy components has been demonstrated. The method, which relies on the recrystallization of a shot-peened surface, needs further development to provide a reliable improvement in fatigue life for beta-processed titanium alloys.

D. References

1. D. Eylon and J. A. Hall, Metall. Trans. A, Vol. 8A, 1977, pp. 981-990.
2. G. R. Leverant, J. E. Hack, and G. P. Sheldon, unpublished research, AFOSR Contract F49620-78-C-0022, Southwest Research Institute, 1979.
3. B. C. Odegard and A. W. Thompson, Metall. Trans., Vol. 5, 1974, pp. 1207-1213.
4. A. W. Thompson and B. C. Odegard, Metall. Trans., Vol. 4, 1973, pp. 899-908.
5. W. J. Evans and C. R. Gostelow, Metall. Trans. A, Vol. 10A, 1979, pp. 1837-1846.
6. D. L. Davidson and D. Eylon, Metall. Trans. A, Vol. 11A, 1980, pp. 837-843.
7. R. R. Boyer and W. F. Spurr, Metall. Trans. A, Vol. 9A, 1978, pp. 23-29.
8. D. A. Meyn, Metall. Trans., Vol. 5, 1974, pp. 2405-2414.
9. N. E. Paton, B. S. Hickman, and D. H. Leslie, Metall. Trans., Vol. 2, 1971, pp. 2791-2796.
10. F. Besel, M.S. Thesis, New York University, New York, NY, 1961.
11. D. F. Neal and P. A. Blenkinsop, Acta Met., Vol. 24, 1976, pp. 59-64.
12. R. J. H. Wanhill, Acta Met., Vol. 21, 1973, pp. 1253-1258.
13. J. Ruppen, P. Bhowal, D. Eylon, and A. J. McEvily, ASTM STP 675, 1979, pp. 47-68.
14. J. E. Hack and G. R. Leverant, Scripta Met., Vol. 14, 1980, pp. 437-441.

15. R. C. Baggerly, N. E. Paton, and J. C. Williams, unpublished research, Rockwell International Science Center, Thousand Oaks, CA, 1976.

16. J. C. M. Li, R. A. Oriani, and L. S. Dar Ken, Z. Phys. Chem., Vol. 49, 1966, pp. 271-290.

17. I. W. Hall and C. Hammond, Met. Sci., Vol. 12, 1978, pp. 339-342.

18. J. P. Hirth and J. Lothe, Theory of Dislocations, McGraw-Hill, Inc., 1968, pp. 696-701.

19. G. Lutjering, Slip Distribution and Mechanical Properties of Metallic Materials, DLR-FB 74-70, Institute for Werkstoff-Forschung, Porz-Wahn, Federal Republic of Germany, 1974.

20. W. R. Kerr, D. Eylon, and J. A. Hall, Metall. Trans. A, Vol. 7A, 1976, pp. 1477-1480.

21. J. C. Williams and N. E. Paton, unpublished research, Rockwell International Science Center, Thousand Oaks, CA, 1973.

22. D. N. Williams, Report on Hydrogen in Titanium and Titanium Alloys, TML Report No. 100, Battelle-Columbus Laboratories, Columbus, OH, May 16, 1958.

23. H. G. Nelson, Hydrogen in Metals, ASM, Metals Park, OH, 1974, pp. 445-464.

III. TITANIUM MATRIX COMPOSITE TASK

D. L. Davidson, R. M. Arrowood, K. Chan,
G. R. Leverant and J. E. Hack

A. Research Objectives

Determine the effect of interfacial strength on the growth of fatigue cracks through a composite of Ti-6Al-4V matrix with continuous fibers of B_4C coated boron.

B. Summary of Research Effort

Matrix/fiber interfacial strength was altered by heat treatment of the composite. Measurements of interfacial shear strength and fiber strength were made, and found to vary systematically with heat treatment. The basis for this effect of heat treatment was investigated by characterizing the interface, both microstructurally and chemically.

The matrix/fiber interface was found by Auger electron spectroscopy to have a relatively high concentration of calcium (8 to 11%). The bigger the combined effect of time and temperature, the larger the concentration of calcium found. Likewise, increasing the interfacial concentration of calcium caused the shear strength decrease. For the heat treatments studied, interfacial shear strength was lowered by a factor of 2-3 times.

Fiber strengths were measured after removing them from the composite. The distribution of fiber strengths was found to be independent of the length of fiber tested; rather, for the two heat treatment conditions examined, fiber strength could be expressed as a percentage of the fibers tested, and this distribution was the same independent of heat treatment, except for the maximum value, Figure 1.

Very detailed analysis of fatigue crack growth through the composite was carried out, with the stereoimaging technique being used to measure crack opening displacement and crack tip strains. In the as-received material, crack tip strains and crack growth rate were found to be highly

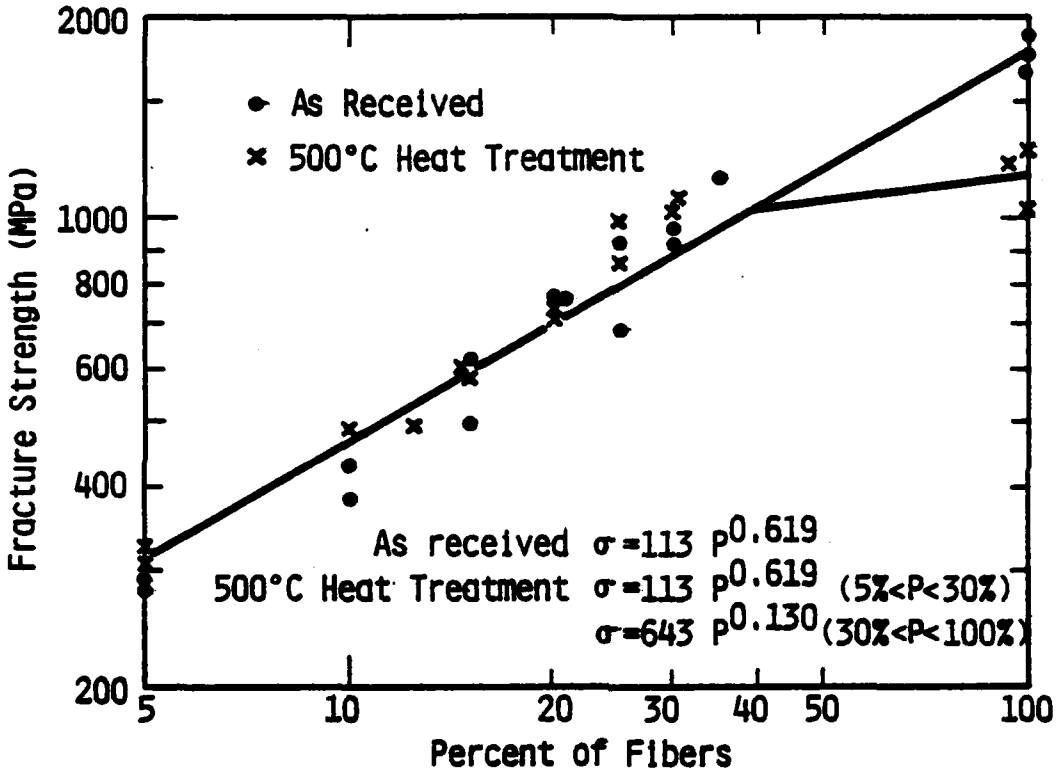

Figure 1. Strength of Fibers as a Percentage of the Total.

dependent upon both the distance of the crack tip from a fiber, and also the integrity of the nearest matrix/fiber interface. Effective cyclic stress intensity factors (ΔK_{eff}) were derived by matching crack tip strains determined using stereoimaging with similar information from fiberless matrix material. Composite crack growth rates for these derived values of ΔK_{eff} were found to match those measured in the composite, Table I.

For heat treated material, the movement of the crack through the composite included considerable crack growth along interfaces, not seen in the as-received material. Fracture of the fibers proved to be a much more erratic process than in the as-received material. This behavior is consistent, however, with the distribution of strengths measured for the fibers. The net result of these changes in crack growth characteristic is that the ΔK below which fatigue cracks will grow is raised for the heat treated material, but the rate of growth of the fatigue crack with increasing ΔK is faster for the heat treated material than for the as-received composite, Figure 2. This means that the rate of crack growth through this composite is sensitive to net section stress. Lateral cracking along the fiber interfaces decreases the importance of the crack tip stress concentration, and increases the significance of net section stress.

Mathematical models have been constructed to describe both the effect of time and temperature of heat treatment on interfacial strength, and the effect of interfacial strength on the rate of fatigue crack growth.

C. Accomplishments

1. Methods have been developed to study quantitatively the effect of interface strength on the rate of fatigue crack growth through a continuous fiber composite.

2. For the composite of Ti-6Al-4V matrix with B_4C coated B fibers, the basis for the lowering of interfacial strength with heat treatment was determined, and the process was mathematically modeled.

TABLE I

EFFECTIVE VALUES OF CRACK GROWTH RATE AND ΔK EXPERIENCED BY CRACKS IN COMPOSITE AT APPLIED ΔK OF 22 $MPa\sqrt{m}$

Location	Maximum Shear Strain	$\Delta K_{eff}(MPa\sqrt{m})$	Equivalent da/dN (μm/cycle)	Observed da/dN (μm/cycle)
Remote from Fiber	.0832	9.4	$2x10^{-2}$	$2x10^{-2}$
Remote from Fiber	.0350	6.6	$4.5x10^{-3}$	$4.5x10^{-3}$
At Debonded Interface	.0299	6.4	$4.5x10^{-3}$	$3.3x10^{-2}$
At Sound Interface	.0240	5.8	$3x10^{-3}$	$3x10^{-3}$

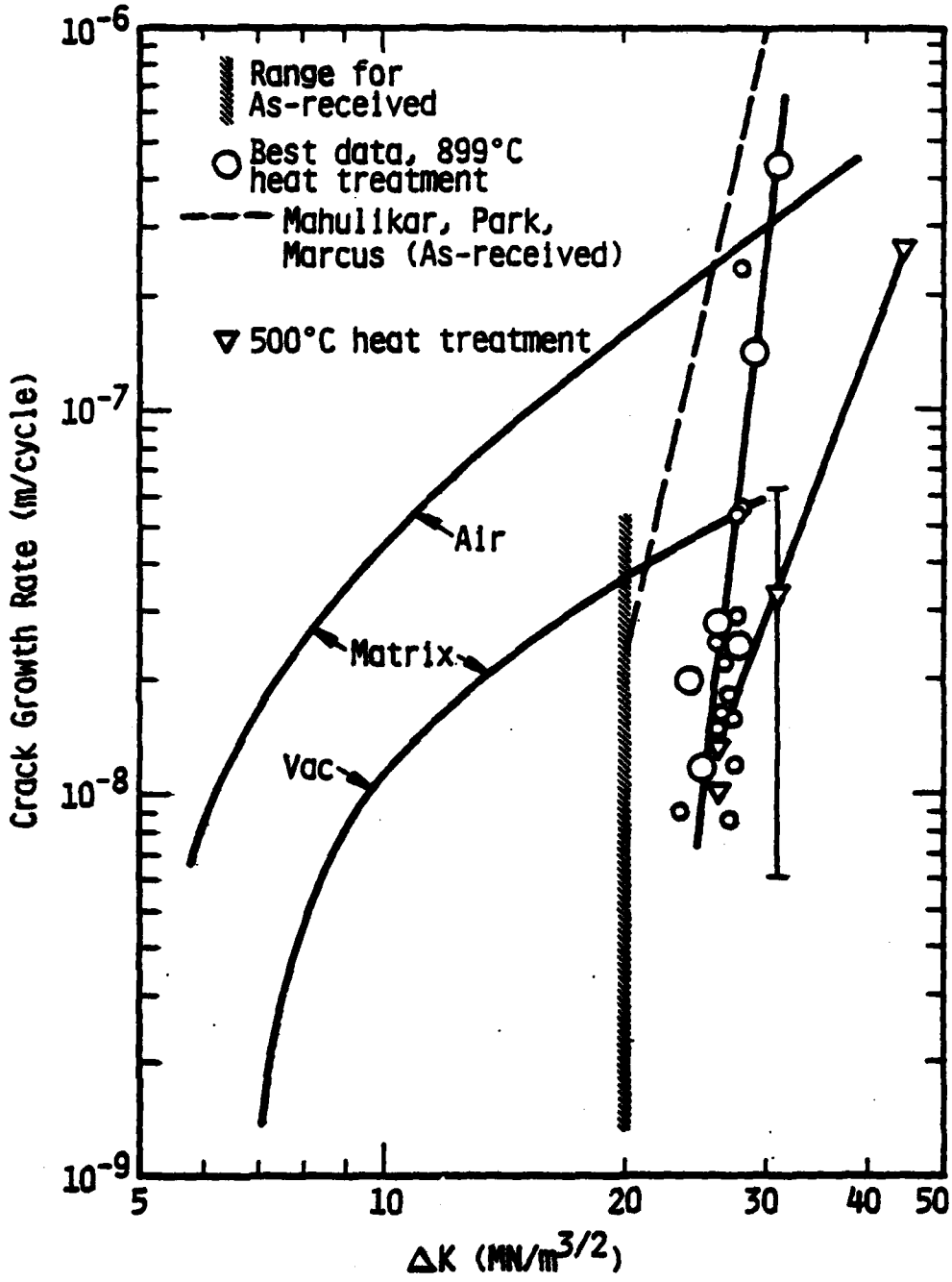

Figure 2. Growth Rate of Fatigue Cracks Perpendicular to the Loading Axis for Both Matrix and Composite.

3. Detailed analysis of the crack opening displacements and crack tip strains for cracks moving through a composite were determined, and from this information the effective driving force (ΔK_{eff}) for crack growth was determined.

4. The effect of heat treatment on fiber strength was determined, as well as a description of the strength of the fibers.

5. A model for crack growth through the composite was derived.

IV. PUBLICATIONS (AFOSR SPONSORSHIP, 1978 THROUGH 1982)

1. J. Lankford and D. L. Davidson, "Fatigue Crack Tip Plastic Zone Sizes in Aluminum Alloys," International Journal of Fracture, 14, p. R87, 1978.

2. D. L. Davidson, "The Study of Fatigue Mechanisms with Electron Channeling," Fatigue Mechanisms, ASTM STP 675, American Society for Testing and Materials, p. 254, 1979.

3. D. L. Davidson, "Fatigue Crack Tip Displacement Observations," Journal of Materials Science, 14, p. 231, 1979.

4. D. L. Davidson and J. Lankford, "Dynamic, Real-Time Fatigue Crack Propagation at High Resolution as Observed in the Scanning Electron Microscope," Fatigue Mechanisms, ASTM STP 675, American Society for Testing and Materials, p. 277, 1979.

5. D. L. Davidson, "The Observation and Measurement of Displacements and Strain by Stereoimaging," SEM/1979, pp. 79-86, 1979.

6. D. L. Davidson and J. Lankford, "Fatigue Crack Tip Plasticity Resulting From Load Interactions in an Aluminum Alloy," Fat. Eng. Mat. Struct., 1, p. 439, 1979.

7. D. L. Davidson and D. Eylon, "Titanium Alloy Fatigue Fracture Facet Investigation by Selected Area Electron Channeling," Met. Trans. A, 11A, pp. 837-843, 1980.

8. D. L. Davidson, "A New Method for Measuring Crack Tip Strains," Inst. of Physics Conf. Series 52 (EMAG'79), Inst. of Physics, London, 1980, pp. 21-24.

9. D. R. Williams, D. L. Davidson, and J. Lankford, "Fatigue Crack Tip Plastic Strains by the Stereoimaging Technique," Experimental Mechanics, 20, p. 134, 1980.

10. D. L. Davidson and J. Lankford, "Fatigue Crack Propagation: New Tools for an Old Problem," Jour. Met., 31, p. 11, 1979.

11. J. Lankford and D. L. Davidson, "Effect of Overloads Upon Fatigue Crack Tip Opening Displacements and Strain Fields in Aluminum Alloys," Fracture 1981, p. 899, 1981.

12. J. E. Hack and G. R. Leverant, "A Model for Hydrogen-Assisted Crack Initiation on Planar Shear Bands in Near-Alpha Titanium Alloys," Scripta Met., 14, p. 437, 1980.

13. D. L. Davidson and J. Lankford, "Characterization of Crack Tip Plastic Zone Parameters and Their Interrelationship with NDE Techniques," Nondestructive Evaluation: Microstructural Characterization and Reliability Strategies, ed. O. Buck and S. M. Wolf, AIME, Warrenville, PA, p. 299, 1981.

14. D. L. Davidson and J. Lankford, "Fatigue Crack Tip Plastic Strain in High Strength Aluminum Alloys," Fatigue of Engineering Materials and Structures, 3, p. 289, 1980.

15. J. E. Hack and G. R. Leverant, "The Influence of Microstructure on the Susceptibility of Near-Alpha Titanium Alloys to Internal Hydrogen Embrittlement," Metallurgical Transactions A, 13A, p. 1729, 1982.

16. D. L. Davidson and J. Lankford, "Fatigue Crack Tip Strains in 7075-T6 by Stereoimaging and Their Use in Crack Growth Models," Quantitative Measurement of Fatigue Damage, ASTM STP 811, 1983 (in press).

17. S. R. Bodner, D. L. Davidson and J. Lankford, "A Description of Fatigue Crack Growth in Terms of Plastic Work," Engineering Fracture Mechanics, 1982 (in press).

18. J. E. Hack, "Comments on 'An Electron Microscope Study of Hydrogen Embrittlement in Vanadium-II'," Scripta Metallurgica, 15, p. 1057, 1981.

19. J. M. Burkstrand, S. P. Clough, D. L. Davidson, and J. E. Hack, "Effects of Thermal Exposure on Fiber-Matrix Interfacial Composition in a Titanium Matrix Composite," in Scanning Electron Microscopy/1982, SEM, Inc. (in press).

20. D. L. Davidson, R. Arrowood, J. E. Hack, and G. R. Leverant, "Micromechanisms of Crack Growth in a Fiber Reinforced Titanium Matrix Composite," to be published, Failure Modes in Composites.

21. D. L. Davidson, "Assessment of Defect Density Magnitude by Changes in Selected Area Electron Channeling Patterns," SEM/1981, SEM, Inc., AMF O'Hare, IL, 1981, pp. 373-387.

22. D. L. Davidson, "Fatigue Crack Plasticity: Dynamic and Static Observations," SESA Annual Conf. Proceedings, pp. 187-189, 1981.

23. D. L. Davidson, "A Model for Relating Crack Opening Displacement and Crack Tip Strain," Scripta Metallurgica, 16, pp. 281-283, 1982.

24. D. L. Davidson, "The Effect of Deformation on Selected Area Electron Channeling Patterns," J. of Mater. Sci. Letters, 1, pp. 236-238, 1982.

25. D. L. Davidson and J. Lankford, "Fatigue Crack Tip Plasticity and Crack Growth Mechanics in Powder Metallurgy and Wrought Aluminum Alloys," Proceedings of: High Performance Aluminum Powder Metallurgy Alloys, TMS-AIME, 1982 (in press).

26. M. E. Fine and D. L. Davidson, "Quantitative Measurement of Energy Associated with a Moving Fatigue Crack," ASTM STP 811, 1983 (in press).

27. J. Lankford and D. L. Davidson, "Characterization of Fatigue Crack Extension Under High Resolution and Dynamic Cycling Conditions," Crack Length Measurement II, ed. C. J. Beevers, 1982 (in press).

28. D. C. Joy, D. E. Newbury, and D. L. Davidson, "Electron Channeling Patterns in the Scanning Electron Microscope," Applied Physics Reviews, Journal of Applied Physics, 53, pp. R81-R122, 1982.

29. J. Lankford and D. L. Davidson, "The Effect of Metallurgical Structure, Environment and Stress Intensity on Fatigue Crack Tip Plasticity in Al-Zn-Mg-Cu Alloys" (in preparation).

30. D. L. Davidson and J. Lankford, "Fatigue Crack Growth Mechanics for Ti-6Al-4V(RA) in Vacuum and Humid Air" (in preparation).

31. D. L. Davidson, R. A. Arrowood, K. Chan, and G. R. Leverant, "The Growth of Fatigue Cracks Through a Titanium Alloy-Boron Fiber Composite," (in preparation) to be submitted to Metallurgical Transactions.

V. PROGRAM PERSONNEL

Name	Title	
Dr. James Lankford	Staff Scientist	
Dr. David L. Davidson	Institute Scientist	Co-principal Investigators
Dr. Gerald R. Leverant	Assistant Director, Materials Sciences	
Mr. John Hack	Senior Research Engineer	
Dr. Roy Arrowood	Senior Research Engineer	
Dr. Kwai Chan	Research Engineer	
Mr. Ronald McInnis	Senior Technician	
Mr. John Campbell	Senior Technician	
Mr. Harold Saldana	Senior Technician	
Mr. James Spencer	Technician	


DATE
ILME